piRNAs safeguard splicing and RNA fidelity during heat shock

Sehee Min, Johnny Cruz-Corchado, and Veena Prahlad*

*corresponding author

Veena.prahlad@roswellpark.org 716-845-8086

Department of Cell Stress Biology

Roswell Park Comprehensive Cancer Center

Elm and Carlton Streets

Buffalo, NY 14263

Keywords: piRNA, heat shock, *hsp,* splicing, nonsense-mediated decay (NMD), endo-siRNAs, transcript fidelity, RNA quality control, protein homeostasis, *C. elegans*

ABSTRACT

Piwi-interacting RNAs (piRNAs) that silence transposons and other non-self-sequences in the genome, also pervasively target endogenous mRNAs in diverse species, and most germline transcripts in *Caenorhabditis elegans*[1-10]. The functions of this broad targeting remain unclear. Here, we uncovered a surprising role for the piRNA pathway in regulating the splicing and fidelity of nascent mRNAs induced during stress. Upon heat shock, piRNAs target essential heat-shock protein (*hsp*) RNAs—normally absent but massively upregulated upon stress—and generate abundant sequence-specific secondary RNAs (22G-RNAs) antisense to these transcripts. Instead of enforcing silencing, these 22G-RNAs associate with nascent *hsp* transcripts and RNA polymerase II at the transcription complex, delaying splicing and preserving a pool of pre-mRNAs for processing during recovery from stress. This role of the piRNA pathway in enforcing splicing delays, extends beyond *hsps* to alternatively spliced genes and ensures the proper expression of long-intron-containing genes in the genome. In piRNA-deficient *prde-1* mutants, splicing is precocious, *hsp* pre-mRNAs are depleted, expression of long-genes is impaired, transcripts accumulate errors, and consequently, embryos become critically dependent on nonsense-mediated decay (NMD) for survival. Downregulating NMD components in piRNA-deficient animals results in the accumulation of polyubiquitinated proteins and embryonic lethality. Thus, by safeguarding splicing under stress, the piRNA pathway complements NMD as a mechanism of RNA quality control, linking RNA fidelity to genome surveillance.

Main

Piwi-interacting RNAs (piRNAs) are small, single-stranded RNA guides for PIWI Argonaute proteins that suppress transposable elements and foreign RNAs through transcriptional and post-transcriptional silencing[1-10]. Yet, across animal species, a large proportion of piRNAs are produced from, and target endogenous genes, suggesting that the piRNA pathway also plays evolutionarily ancient and conserved roles in regulating gene expression[1-7,11-15]. However, their endogenous functions remain mostly unknown. In *Caenorhabditis elegans*, piRNAs associate with PRG-1 (the *C. elegans* PIWI protein) and can target, with high mismatch tolerance, nearly all germline RNAs, including ectopic sequences such as GFP transgenes[1,2,16,17]. piRNA-targeting initiates the production of secondary antisense small endogenous silencing RNAs (endo-siRNAs, or 22G-RNAs) templated from the piRNA-targeted mRNAs by RNA-dependent RNA polymerases (RdRPs)[18-20]. These 22G-RNAs recruit WAGO Argonaute proteins to enforce co- and post-transcriptional silencing. Self-RNAs are spared this promiscuous silencing through their interactions with another Argonaute protein, CSR-1, guided by 22G-RNAs generated from actively translated transcripts independently of piRNAs[21,22]. These CSR-1 associated 22G-RNAs, thus, act as molecular engrams that recognize expressed 'self' genes to prevent their silencing. However, this leaves unexplained how inducible genes such as heat shock protein (*hsp*) genes—normally absent and thus lacking CSR-1-22G-RNA guides, but whose abrupt and massive expression is essential to ensure survival under heat shock and other stress[23-25] — escape piRNA-mediated silencing.

hsp mRNAs are targeted by the piRNA pathway

To address this question, we performed small RNA (sRNA-seq) and mRNA (paired-end, strand-specific, polyA-selected) sequencing from synchronized day-one adults exposed to mild (5 mins, 34°C) or strong (30 mins, 34°C) heat shock (Suppl. Fig 1a; Suppl. Tables 1, 2). Animals were also analyzed after two hours of recovery at 20°C, when normal physiological functions largely

65 resume[26]. In parallel, to identify piRNA-dependent effects, we sequenced *prde-1* mutants,
66 deficient in piRNA biogenesis[27,28] (Suppl. Fig. 1a; Suppl. Tables 1, 2). As expected, heat shock
67 induced global changes in mRNA (Suppl. Fig 1b), including the massive upregulation of *hsp* genes
68 (Fig 1a; Suppl. Fig 1c, d *mRNA*). Surprisingly, in wild-type animals, heat shock also produced
69 22G-RNAs antisense to the *hsp* mRNAs (Fig 1a; Suppl. Fig 1c, d *22G-RNA*), suggesting that
70 rather than escaping piRNA surveillance, *hsp* mRNAs may be targeted by the piRNA system. Like
71 the *hsp* mRNAs, these antisense 22G-RNAs also appeared within 5 minutes of heat shock and
72 peaked during recovery (Fig 1a; Suppl. Fig 1c, d *22G-RNA*). Consistently, by 30 minutes of heat
73 shock, several piRNAs were also modestly but significantly induced (Suppl. Fig 1e, f). In *prde-1*
74 mutants, *hsp* induction upon heat shock was intact, but many fewer 22G-RNAs antisense to *hsp*
75 mRNAs were produced (Fig 1a; Suppl. Fig 1c, d *mRNA; 22G-RNA*), further suggesting that these
76 22G-RNAs were generated because of piRNA-targeting.
77
78 Because *hsp* expression is essential for stress survival, and piRNA targeting typically enforces
79 silencing through the PIWI Argonaute PRG-1[16,19], to confirm these unexpected results, we tested
80 whether *hsp* mRNAs interact with PRG-1. PRG-1 and RdRPs reside in perinuclear condensates
81 (nuage or germ granules) of the germline, where piRNA-induced 22G-RNAs are also produced
82 [29,30]. Heat shock induced the expression of *hsp* mRNA in the germline: RNA Fluorescence *in situ*
83 hybridization (RNA FISH) showed that *hsp-70s (C12C8.1* and *F44E5.4/.5)* were induced by (and
84 only by) late pachytene nuclei (Fig 1b, c; Suppl. Fig 2a). PRG-1 was expressed in these regions.
85 Moreover, although PRG-1 localization is known to dissolve upon exposure to increased
86 temperatures, PRG-1 remained in perinuclear condensates upon heat shock, in these pachytene
87 nuclei (Fig. 1b, d; compare transition zone, TZ, where *hsp* mRNAs are absent, with Pachytene).
88 Immunoprecipitating PRG-1 under control, heat-shock, and recovery conditions from animals
89 expressing FLAG-tagged PRG-1 showed that *hsp-70 (C12C8.1* and *F44E5.4/.5)* mRNAs
90 associated with PRG-1 (RNA immunoprecipitation, RIP, followed by RT–qPCR; Fig 1e, f). Non-

91 FLAG animals were used to account for non-specific interactions of *hsp* mRNAs, and *bath-45,* a
92 known piRNA target, served as a positive control (Fig 1e, f; Suppl. Fig 2b). In addition, and most
93 convincing, depleting PRDE-1 specifically in the germline using an auxin-inducible degron (AID)
94 system abolished 22G-RNAs presence throughout the animal (RNA FISH), demonstrating that
95 22G-RNAs originate in the germline through piRNA targeting (Fig 1g, h; embryos show non-
96 specific staining). Surprisingly, despite their germline origin, the 22G-RNAs were present
97 throughout the animal, in somatic cells that expressed *hsp* mRNA (e.g. muscle, somatic sheath
98 cells), as well as in the germline cells such as sperm, which do not (RNA FISH; Fig 1g, h; Suppl.
99 Fig 2c). Upon germline depletion of PRDE-1, 22G-RNA levels were starkly decreased in somatic
100 and germline cells (Fig 1g, h), while *hsp-70* mRNA continued to be expressed (Suppl. Fig 2c).
101 Together, these findings confirmed that *hsp* mRNAs were subject to piRNA surveillance, actively
102 targeted by the canonical piRNA pathway in the germline, and produced 22G-RNAs that
103 propagated systemically across tissues.
104
105 Further evidence that the *hsp* genes induced by heat shock were templating antisense 22G-RNA
106 production came from profiling mRNAs and sRNAs in a mutant in heat shock factor 1 (HSF1;
107 HSF-1 in *C. elegans*), the transcription factor responsible for *hsp* expression upon heat shock.
108 This mutant, *hsf-1 (sy441)* is deficient in heat-induced activity but expresses higher basal levels
109 of *hsp* mRNA[26,31] . Yet *hsf-1* mutants failed to produce 22G-RNAs antisense to *hsp* genes (Fig 1a;
110 Suppl. Fig 1c, d). Surprisingly, even the few *hsp* mRNAs, like *hsp-70 (F44E5.4/.5)*, that did
111 accumulate upon heat shock in *hsf-1 (sy441)* mutants, did not template 22G-RNAs (Suppl. Fig
112 1c, d), perhaps suggesting a broader role for HSF-1 in piRNA-dependent 22G-RNA production.
113 piRNA surveillance also extended beyond *hsps* to other heat-shock-regulated genes: ~15% of
114 differentially expressed genes (DEGs) upon a 5-minute heat-shock and ~40% by 30 minutes
115 templated 22G-RNA production, and both the numbers of DEGs, and DEG-derived 22G-RNAs
116 were reduced in *prde-1* and *hsf-1* mutants (Fig 1i; Suppl. Fig 2d; Suppl. Table 3). 22G-RNA

117 function is determined by its Argonaute partner; however, the 22G-RNAs that targeted *hsp*
118 mRNAs were 'unclassified' and not previously identified in association with known *C. elegans*
119 Argonaute proteins (Suppl. Fig 3; Suppl. Table 3). However, DEGs other than the *hsp* genes, did
120 template 22G-RNAs that had been previously identified as guide RNAs for WAGO, CSR-1 and
121 other Argonaute proteins (Suppl. Table 4). WAGO-associated 22G-RNAs that were induced upon
122 30 minutes of heat shock exposure were piRNA-dependent, as apparent by their decreased levels
123 in *prde-1* mutants, and in wild-type they increased as their target mRNAs decreased, consistent
124 with their known roles in post-transcriptional or co-transcriptional silencing[8,32] (Suppl. Fig 3a, b).
125 CSR-1 22G-RNAs declined upon heat shock (perhaps due to translational attenuation), as their
126 target mRNAs rose in both wild type and *prde-1* mutants, consistent with their mostly piRNA-
127 independent production (Suppl. Fig 3a, b). Unclassified 22G-RNAs continued to increase in a *hsf-*
128 *1-* and *prde-1-* dependent manner, even during recovery from heat shock, as did their
129 complementary mRNAs (Suppl. Fig 3a, b). The effects were dynamic and reversible during
130 recovery from stress (Suppl. Fig 2d (Rec); Suppl. Fig 3a, b), and the mRNAs that templated 22G-
131 RNA production showed distinct GO enrichments (Suppl. Fig 4; Suppl. Table 5), suggesting that
132 the broad piRNA-dependent and independent 22G-RNA expression that was triggered by heat
133 shock likely contributes to the pervasive transcriptome-wide remodeling[8,32] universally associated
134 with this stress-induced transcription program.
135

136 **The piRNA-pathway regulates post-transcriptional splicing.**

137 Given the known roles of piRNAs in post- and co-transcriptional silencing, we suspected that
138 piRNA targeting of *hsp* and other stress-induced genes functioned to clear transcripts during
139 recovery from heat shock. If so, *hsp* mRNAs should persist longer after stress in *prde-1* mutants.
140 Instead, RT-qPCR (Suppl. Fig 5a-c) and RNA-FISH (Suppl. Fig 5d) revealed the opposite: the
141 steady state abundance of *hsp* mRNAs declined more rapidly in *prde-1* mutants compared to wild
142 type. We examined whether decreased RNA Polymerase II (Pol II) binding at *hsp* genes[33], or

143 altered transcription duration, explained this progressive decline. But this was also not the case:
144 chromatin immunoprecipitation followed by qPCR (ChIP-qPCR) showed that Pol II levels at *hsp*
145 gene transcription start sites (TSS), and its return to basal levels by 2 hours post-heat shock,
146 were similar in *prde-1* and wild-type animals (Suppl. Fig 5e, f). Therefore, to understand the role
147 of the piRNA pathway's targeting of *hsps* and other heat-shock genes, we directly assessed *hsp*
148 mRNA dynamics in the absence and presence of the piRNA pathway by its synthesis and turnover
149 using a pulse-chase metabolic labeling approach: we labeled the heat-shock induced pre-mRNA
150 with 5-ethynyluridine (EU)[34,35] provided to the animals only during heat shock exposure, and
151 tracked the fate of this RNA during recovery from heat shock by absolute RT–qPCR using exon–
152 intron (pre-mRNA) and exon–exon (mature mRNA) primers (Fig 2a; see methods for experimental
153 details). Consistent with similar Pol II occupancy at *hsp* genes, *prde-1* synthesized similar total
154 amounts of RNA as wild-type animals upon heat shock (Suppl. Fig 5g, h). Despite this, *prde-1*
155 mutants had significantly reduced amounts of nascent (EU-labeled) pre-mRNA by the end of the
156 30-minute heat shock (Fig 2b; Suppl. Fig 5i), but, on the other hand, accumulated significantly
157 more EU-containing spliced mRNA by 2 hours following heat shock (Fig 2c; Suppl. Fig 5j). This
158 suggested that in the absence of piRNAs, *hsp* splicing or maturation occurred at an accelerated
159 pace, resulting in a precocious increase in nascent mRNAs and a concomitant decrease in pre-
160 mRNA pools.
161
162 The amounts of unspliced nascent pre-mRNA present at the end of heat shock exposure,
163 calculated as the ratio of EU-labeled pre-mRNA over total EU-labeled RNA[36], also indicated that
164 piRNA/22G-RNAs functioned to delay splicing in wild-type animals. In the presence of
165 piRNAs/22G-RNAs, in wild-type animals, ~75% of nascent *hsp-70 (C12C8.1)* transcripts, which
166 contain two introns, remained as pre-mRNA to be spliced post-transcriptionally during recovery
167 (Fig 2d). In contrast, only ~57% persisted unspliced in *prde-1* mutants (Fig 2d), suggesting that
168 the piRNA pathway was biasing the decision between co- and post-transcriptional splicing to favor

169 delayed splicing. This remaining *hsp-70 (C12C8.1)* was also spliced more rapidly in *prde-1*
170 animals: within 2 hours of recovery, dramatically more EU-containing spliced mRNAs were
171 produced from the nascent EU-labeled unspliced pre-mRNA (Fig 2e). The other inducible *hsp-70*
172 *(F44E5.4/.5)*, contained only one intron, and was mainly co-transcriptionally spliced in both wild-
173 type and *prde-1* animals (Suppl. Fig 5k). Still, the post-transcriptional splicing of the residual *hsp-*
174 *70 (F44E5.4/.5)* proceeded markedly faster in *prde-1* mutants than in wild-type animals (Suppl.
175 Fig 5l). This was also true for the small heat shock protein (*hsp-16.11*; Suppl. Fig 5m).
176
177 The accelerated splicing rates in *prde-1* mutants were not simply due to altered expression of
178 protein coding genes. We could rescue *hsp* RNA dynamics — both the persistence of *hsp* mRNA
179 (Fig 2g), and the levels of *hsp* pre-mRNA in heat-shocked *prde-1* animals (Fig 2h) by
180 microinjecting *prde-1* animals with only the heat-shock-induced small RNA fraction (<200nt)
181 obtained from wild-type, but not *prde-1* animals, shortly prior to heat shock exposure. Small RNA
182 injections *per* se did not induce or enhance *hsp* expression (Fig 2g, h). Thus, global alterations in
183 mRNAs were unlikely to be responsible for the differences in splicing rates in *prde-1* animals, and,
184 together with the results from pulse-chase metabolic labeling, these results showed that the
185 piRNA/22G-RNA pathway functioned dynamically, preserving mRNA expression during heat-
186 shock recovery by restraining splicing and maintaining a pool of pre-mRNAs for delayed
187 processing.
188
189 Heat shock and other stressors lead to genome-wide splicing inhibition, intron retention, and
190 retention of unspliced RNAs in chromatin [36-40]. We therefore analyzed our RNA-seq data to assess
191 whether the piRNA pathway was responsible for intron retention or alternative splicing (AS) of
192 genes other than *hsps*, leveraging previous studies demonstrating introns in poly(A)+ selected
193 mRNAs[36,41,42]. In wild-type animals, heat shock-DEGs (p.adj <0.05) were enriched for AS isoforms,
194 and had significantly more transcript isoforms than DEGs in *prde-1,* as indicated by their much

195 lower "percent spliced in" (PSI or Ψ)[43,44] values (Fig 2i). In addition, 540 transcripts showed
196 significant dPSI (differential PSI; p <0.1) values, compared to only 139 transcripts in *prde-1* (Suppl.
197 Table 6). Moreover, for seven representative AS events[45,46] — retained intron (RI), alternative 5'/3'
198 Splice Sites (A5/A3), skipped exon (SE), mutually exclusive exons (MX), and alternative first and
199 last exons (AF/AL) (Fig 2j) — mRNAs differentially expressed upon heat shock in wild-type
200 animals were significantly less spliced, retaining more introns compared to *prde-1* (Fig 2j; Suppl.
201 Table 7). Nearly 40% (125/308) of these genes that produced AS transcripts upon heat shock in
202 wild-type animals templated 22G-RNAs, compared to only 12% (35/280) in *prde-1* (Suppl. Fig 6a).
203 These AS mRNAs were enriched in developmental processes, and in particular in neuronal
204 functions known to rely on AS (Suppl. Fig 6b; Suppl. Table 8), suggesting that their delayed
205 splicing may be important for the restoration of developmental processes during recovery from
206 heat shock, and accordingly, heat-shocked *prde-1* mothers showed a marked delay in generating
207 viable embryos post-heat shock (Suppl. Fig 6c, d).
208
209 **22G-RNAs act through a 'telescripting'-like mechanism to protect long gene expression.**
210 Mechanistically piRNA/22G-RNAs could regulate splicing indirectly, through their known
211 interactions with chromatin[8,29,47]. Alternatively, and consistent with the rapid induction and splicing
212 of *hsp* genes, they could regulate splicing directly by acting on target pre-mRNAs at the
213 transcription complex to bias splicing decisions[39]. Therefore, to understand how 22G-RNAs
214 regulate splicing, we adapted Photoactivatable Ribonucleoside-Enhanced Crosslinking and
215 Immunoprecipitation (PAR-CLIP) to test whether these small RNAs are associated with Pol II at
216 the transcription complex. While co-transcriptional splicing occurs in association with elongating
217 Pol II, post-transcriptional splicing is thought to occur after the pre-mRNA is released from Pol II,
218 but the mechanisms that regulate the timing, transition, and completion of splicing are unclear[48,49] .
219 Therefore, taking advantage of the fact that 4sU, like EU, is primarily incorporated into nascent
220 RNAs, we also assessed if *hsp* mRNA and/or pre-mRNA associated with Pol II, by

221 immunoprecipitating Pol II, immediately at 30 minutes upon heat shock, when transcription was
222 still in process, or after 2 hours of recovery from heat shock, when Pol II was no longer engaged
223 with the *hsp* locus (ChIP-qPCR; Suppl. Fig 5e, f), but spliced mRNAs accumulated (Fig 2c; Suppl.
224 Fig 5j).
225
226 Animals were fed 4-thiouridine (4sU) at non-inhibitory concentrations (Fig 3a; Suppl. Fig 7a, b),
227 subjected to heat shock, exposed to UV (365 nm) to crosslink nascent RNA to Pol II at the
228 described time points, Pol II was immunoprecipitated, and the RNA species associated with Pol
229 II identified using absolute and stem-loop RT-qPCR. In wild-type animals, as expected, unspliced
230 *hsp* pre-mRNAs co-immunoprecipitated with Pol II at 30 minutes after heat shock, decreasing by
231 2 hours post-heat shock recovery (Fig 3b; Suppl. Fig 7d). Nevertheless, a small but significant
232 fraction of nascent pre-mRNA remained associated with Pol II 2 hours post-heat shock (Fig 3b;
233 Suppl. Fig 7d), when Pol II was no longer transcriptionally engaged (ChIP-qPCR; Suppl. Fig 5e,
234 f). Notably, 22G-RNAs antisense to *hsp-70* (*C12C8.1*) also co-immunoprecipitated with Pol II, 2
235 hours post-heat shock (Fig 3c), as concomitantly, increasing amounts of *hsp-70* mRNA were
236 spliced, and also associated with Pol II (Fig 3d). Furthermore, chromatin fractionation showed
237 that these progressively increasing spliced mRNAs were retained in chromatin (Fig 3e, f). In *prde-*
238 *1* mutants, less pre-mRNA (Fig 3b), but more constitutively spliced nascent mRNA (Fig 3d) was
239 associated with Pol II at 30 minutes heat shock, and 22G-RNAs were not present (Fig 3c). In
240 addition, spliced *hsp-70* mRNA failed to increase on chromatin (Fig 3e, f), or in association with
241 Pol II above these basal constitutive levels (Fig 3d), instead appearing to be efficiently exported
242 and translated as seen by elevated HSP-70 protein levels (Fig 3g).
243
244 A broadly similar dynamic was observed with *hsp-70 (F44E5.4/.5)*, even though the majority of
245 RNA was already spliced, co-transcriptionally (Suppl. Fig 5k). Here, by the end of 30 minutes of
246 heat shock, the remaining amounts of pre-mRNA that associated with Pol II were not significantly

247 different between wild-type and *prde-1* animals (Suppl. Fig 7d), but significantly more mRNA was
248 crosslinked with Pol II in wild-type animals (Suppl. Fig 7e), remained associated with Pol II during
249 recovery (Suppl. Fig 7e), and accumulated in chromatin (Suppl. Fig 7f). Also, like with *hsp-70*
250 *(C12C8.1)*, significantly more 22G-RNA associated with Pol II in wild-type animals compared to
251 *prde-1* (Suppl. Fig 7g). Perhaps due to the difference in splicing strategy between the two *hsp-*
252 *70s*, 22G-RNA kinetics in association with Pol II varied: at 30 minutes upon heat shock, 22G-RNA
253 associated with Pol II decreased in *prde-1*, rather than increasing in wild-type. Notwithstanding
254 these differences, these data together showed that the piRNA-generated 22G-RNAs act at the
255 transcription complex, associating with Pol II, to delay splicing, and promote chromatin retention
256 of *hsp* mRNAs, postponing the availability of *hsp-70* mRNAs for translation. The continued
257 association of unspliced and spliced RNAs along with 22G-RNAs with Pol II after transcription
258 was complete and Pol II had disengaged from the *hsp* genes — most evident in *hsp-70 (C12C8.1)*,
259 where a larger fraction underwent post-transcriptional splicing — also suggested that post-
260 transcriptional splicing of *hsp* RNA occurs in direct or indirect association with Pol II.
261
262 The ability of antisense 22G-RNAs to retard splicing at the transcription complex through
263 association with Pol II and nascent pre-mRNA was reminiscent of mechanisms by which U1
264 snRNA base-pairs with nascent transcripts to modulate their splicing efficiency and rates, and
265 initiates telescripting, a process that prevents premature transcription termination, particularly of
266 long-intron containing genes[50-52]. In mammalian cells, heat shock decreases U1 snRNA levels,
267 resulting in the loss of telescripting and a decrease in the expression of long-intron-containing
268 genes[53,54]. Like mammalian cells, *C. elegans*, also showed a modest but significant decrease in
269 at least three of five U1 snRNAs tested (Fig 3h; Suppl. Fig 7h). Yet, unlike mammalian cells, in
270 wild-type *C. elegans,* despite reduced U1 RNA levels, genes upregulated upon heat shock were
271 preferentially enriched for long-intron-containing genes. This was visible in the increase in their
272 average gene lengths (Fig 3i) and the cumulative distribution plots of gene lengths of differentially

273 upregulated and downregulated genes (p.adj <0.05) (Suppl. Fig 8a), and metagene profiles of
274 expression values of all expressed genes segregated by gene length (Suppl. Fig 8b, c; Suppl.
275 Table 9). *prde-1* animals showed a marked deficiency in upregulating long genes, although they
276 did not differ from wild-type in downregulation of long genes (Fig. 3i, Suppl. Fig 8a; also see Suppl.
277 Fig 8b, c). This raised the intriguing possibility that the 22G-RNAs generated by wild-type animals
278 were functionally substituting for U1 snRNAs during stress, ensuring productive Pol II elongation
279 and expression of long-intron-containing genes. In support of this, ChIP–qPCR showed that
280 elongating Pol II (S2P) levels were markedly and significantly decreased at *hsps (C12C8.1* and
281 *F44E5.4/.5)* 3′ ends in *prde-1*, despite normal occupancy at the 5′-end, mirroring phenotypes
282 caused by disrupting U1–nascent RNA interactions[51,52] (Fig 3j; Suppl. Fig 8d).
283
284 Together, these findings indicate that the piRNA pathway delays splicing and promotes chromatin
285 retention of mature mRNAs by associating with the transcription complex. In doing so, the
286 antisense 22G-RNAs act in a manner strikingly similar to U1 telescripting: both systems protect
287 splicing, preserve Pol II elongation, and the expression of long-intron containing genes, essential
288 for development.
289
290 **The piRNA pathway preserves transcript fidelity and complements nonsense-mediated**
291 **decay as a mechanism enforcing RNA quality control.**
292 The accelerated splicing observed in *prde-1* mutants, even under heat shock conditions when
293 spliceosome function is challenged, and reduced RNA polymerase II occupancy at the 3′ ends of
294 *hsp* genes (Fig 3j, Suppl. Fig 8d), suggested to us that in the absence of piRNAs, mRNA
295 transcripts may accumulate errors due to aberrant splicing or premature termination. To directly
296 test this hypothesis, we used Unique Molecular Identifiers (UMIs)[55-59] to label individual mRNAs
297 from heat-shocked wild-type and *prde-1* mutants and selected single mRNA molecules (free of
298 PCR amplification artifacts) to analyze for the accumulation of transcript variants or 'errors' (**Suppl.**

299 **Online Material).** To generate an 'error rate', we mapped the individual RNAs onto the *C.elegans*
300 reference genome, excluded SNPs that could be attributed to potential genomic changes due to
301 the *prde-1* mutation (see Methods for details), and identified high quality variant containing sites
302 using the program Genome Analysis Toolkit (GATK), as regions where one or more mRNAs
303 contained mismatches or misalignments when compared to the reference genome. To increase
304 our confidence that any mismatches were 'errors', we further selected regions with a minimum
305 coverage > 10 reads. We then determined the fraction of mRNAs in wild-type and *prde-1* animals
306 that contained these mismatches (see Methods and Suppl. Table 10). Amongst the approximately
307 2.7×10^7 individual mRNAs, we identified 2045-2054 variant containing sites, and of these, a
308 larger fraction of mRNAs in *prde-1* mutants had one or more variants (Suppl. Fig 9a; p.adj =
309 0.133). This was particularly true when we analyzed nonsense, missense, and frameshift
310 variants, called by the program SnpEff (Fig 4a; p.adj <0.05). Notably, the *prde-1* variant mRNAs
311 were not uniformly distributed across the genome; instead, they were disproportionately enriched
312 in mRNAs from smaller genes, which were also more highly expressed by *prde-1* (Fig 4b; also
313 see Suppl. Fig 8c). Amongst the base changes G>A was the most highly represented (Fig 4c),
314 consistent with the increased error rates associated with misincorporation of faster-incorporating
315 bases by Pol II[60]. This suggested that the splicing delay imposed by the piRNA pathway protected
316 transcript fidelity under stress, and in its absence, animals may be accumulating more 'errors' in
317 their transcripts. However, this analysis did not exclude the possibility that these variants
318 represented RNA modifications or increased RNA-editing in the *prde-1* animals.
319
320 Therefore, to independently evaluate whether *prde-1* animals accumulated more splicing errors,
321 we examined whether they were more susceptible to the downregulation of the nonsense-
322 mediated mRNA decay (NMD) pathway, a system that surveils and eliminates transcripts that are
323 unproductively spliced[61-66]. Remarkably, downregulating *smg-1*, the NMD kinase, resulted in the
324 complete loss of viability of *prde-1* embryos, not only upon heat shock but also under control

325 conditions (Fig 4d-f). Downregulating *smg-2* (homolog of UPF1)[67] and *smg-3* (homolog of UPF2)[67]
326 in parents also resulted in complete or partial loss of viability in their embryos, again even under
327 control conditions (Fig 4e), or if parents were subjected to heat shock (Fig 4f). In contrast, wild-
328 type embryos were not affected by *smg-1, smg-2, smg-3* RNAi, under either heat shock or control
329 conditions (Fig 4d-f), consistent with previous studies showing that NMD is not required for *C.*
330 *elegans* survival[61,67,68]. The involvement of NMD suggested that the mis-transcribed mRNA in
331 *prde-1* was likely being eliminated during translation. In support of this, in the absence of *smg-1*,
332 *prde-1* animals accumulated significantly higher amounts of polyubiquitinated proteins even under
333 control conditions, in the absence of proteotoxic stress (Fig 4g; see methods for how viable *smg-*
334 *1*-RNAi-treated *prde-1* were obtained). Taken together these studies suggest that piRNAs and
335 NMD act in complementary modes of RNA quality control: piRNAs delay splicing to preserve
336 accurate pre-mRNAs under stress, while NMD serves to eliminate erroneous transcripts when
337 this buffering mechanism is lost (Fig 4h).
338
339 **Discussion.**
340 In summary, using *hsp* mRNAs as the paradigmatic model for inducible gene expression, we
341 uncovered a surprising role for the piRNA pathway in regulating splicing during the heat shock
342 response, when spliceosome activity is compromised[36,37,53]. We found that upon heat shock,
343 newly induced *hsp* mRNAs become targets for piRNA surveillance, rapidly becoming associated
344 with PIWI (PRG-1) and producing piRNA-induced antisense 22G-RNAs. These 22G-RNAs
345 interact with RNA polymerase II and nascent *hsp* pre-mRNAs to regulate splicing and delay
346 transcript maturation and translation. Remarkably, this piRNA-dependent mechanism is
347 necessary to safeguard mRNA fidelity. In the absence of piRNAs, splicing is accelerated, leading
348 to transcript errors and increased dependence on NMD. Thus piRNA-regulation of splicing
349 complements NMD as an RNA quality control mechanism.
350

351 Our studies also suggest that the function of the piRNA pathway extends beyond *hsp* genes to
352 regulate alternative splicing, and the expression of long genes, many of which also template 22G-
353 RNAs during stress. The 22G-RNAs that modulate *hsp* splicing are part of a larger population of
354 piRNA- and *hsf-1*- dependent 'unclassified" 22G-RNAs, whose levels increase during recovery
355 from heat shock along with their complementary mRNA targets, suggesting that this pool of endo-
356 siRNAs may mark post-transcriptionally spliced or processed genes, although this remains to be
357 shown. Also, we are yet to identify the detailed mechanisms of splicing regulation. Still, the
358 similarities to U1 RNA-mediated splicing and telescripting[50-54] are striking: both systems use base-
359 pairing of noncoding RNAs to stabilize nascent transcripts, bias splicing, stabilize pre-mRNAs,
360 prevent the premature loss of elongating Pol II from the 3' end of genes, and protect the
361 expression of long-intron-containing genes. These parallels raise the intriguing possibility that,
362 analogous to therapeutic antisense oligonucleotides explored for clinical applications, *C. elegans*
363 may employ piRNA/22G RNAs as a natural small RNA–guided telescripting system to substitute
364 for, or complement, U1 RNAs for RNA splicing. Post-transcriptional control of gene expression is
365 emerging as a critical mechanism to regulate development, stress, and phenotypic plasticity[39,48].
366 Yet, how cells select transcripts for delayed splicing, how such delays are mechanistically
367 implemented, and if and how splicing decisions are coordinated across the diverse tissues is
368 poorly understood. The sequence complementarity of 22G-RNAs to expressed exonic regions of
369 mRNAs, and their responsiveness to transcriptional and translational events within the cell, might
370 allow them to act as flexible modulators of splicing decisions.
371
372 Several cell-autonomous activities of small RNAs, including piRNAs have been described, across
373 species, and in *C. elegans*. These include post-transcriptional gene silencing through RNA
374 cleavage, RNA decay, translation repression, transcriptional gene silencing through inhibition of
375 RNA polymerase II (Pol II)-mediated transcript elongation and cDNA or histone methylation[5-7,69,70].
376 Only very few previous studies have linked the piRNA pathway to splicing regulation[71,72]. Yet,

377 these studies suggest that the piRNA-splicing-regulation, and its functions may be conserved
378 across species. Thus, in *Drosophila*[71] nuclear Piwi complexes inhibit splicing of the *gypsy*
379 retrotransposon through chromatin-based, co-transcriptional silencing, whereas in locusts[72]
380 piRNAs facilitate splicing of specific pre-mRNAs during oocyte maturation, suggesting both
381 inhibitory and stimulating role for piRNAs in splicing control. Intriguingly, in *C. elegans*, the
382 presence of introns protects transcripts from default Argonaute-mediated silencing in the germline,
383 and the WAGO Argonaute, HRDE-1 have been shown to interact with the conserved RNA
384 helicase Aquarius/EMB-4[73-75], further implicating piRNA function in RNA splicing regulation. In our
385 studies, the 22G-RNAs appear capable of crossing cell boundaries, suggesting a potential role in
386 coordinating splicing across tissues. Also, remarkably, the 22G-RNAs antisense to *hsp* mRNAs
387 were enriched in sperm, an observation that parallels the presence of piRNAs in mature
388 mammalian sperm[76], where they are thought to influence sperm quality, motility, and epigenetic
389 inheritance.
390
391 In *C. elegans*, loss of the piRNA pathway leads to a sporadic, and temperature-dependent
392 increase in infertility over time, a defect that can be mitigated by slowing growth or metabolism[9,77].
393 In addition, NMD, which mainly silences pseudogenes, is crucial for longevity[78,79]. Thus, our
394 findings suggest that, similar to aging-dependent neurodegenerative disorders, the increased
395 infertility upon piRNA loss may be due to the progressive accumulation of RNA errors arising from
396 the loss of piRNA-control over splicing rates, and increased misfolded proteins due to an
397 overwhelmed NMD system. Taken together with the known roles of piRNAs in transposon and
398 pseudogene regulation of germline mRNAs, and the growing evidence for links between splicing,
399 genome stability, and transposon activation[80], our findings suggest that piRNAs pathway may
400 serve as a conserved node to integrate genome surveillance with RNA and protein quality control.

401 **Acknowledgements**

402 We thank Ms. Selvarasu for microinjection experiments, the V.P. laboratory, Drs. Josep Comeron
403 and Anna Malkova and Ana Llopart for comments, Rochester Genomics Research Center for
404 small RNA sequencing and advice, Drs. Paul Quinn and Prashant Singh for mRNA-sequencing,
405 UMI libraries and advice, and Caenorhabditis Genetics Center (CGC) (funded by the NIH
406 Infrastructure Programs P40 OD010440) for *C. elegans* strains. This work was supported by NIH
407 R01 MH126282 (V.P.), and support for the sequencing core from the National Cancer Institute
408 (NCI) grant P30CA016056 to the Roswell Park Comprehensive Cancer Center.

409 **References**

410

411 1 Shen, E. Z. *et al.* Identification of piRNA Binding Sites Reveals the Argonaute Regulatory
412 Landscape of the C. elegans Germline. *Cell* **172**, 937-951 e918 (2018).
413 https://doi.org:10.1016/j.cell.2018.02.002

414 2 Lee, H. C. *et al.* C. elegans piRNAs mediate the genome-wide surveillance of germline
415 transcripts. *Cell* **150**, 78-87 (2012). https://doi.org:10.1016/j.cell.2012.06.016

416 3 Gainetdinov, I. *et al.* Relaxed targeting rules help PIWI proteins silence transposons.
417 *Nature* **619**, 394-402 (2023). https://doi.org:10.1038/s41586-023-06257-4

418 4 Wu, P. H. & Zamore, P. D. Defining the functions of PIWI-interacting RNAs. *Nat Rev Mol*
419 *Cell Biol* **22**, 239-240 (2021). https://doi.org:10.1038/s41580-021-00336-y

420 5 Czech, B. *et al.* piRNA-Guided Genome Defense: From Biogenesis to Silencing. *Annu*
421 *Rev Genet* **52**, 131-157 (2018). https://doi.org:10.1146/annurev-genet-120417-031441

422 6 Ozata, D. M., Gainetdinov, I., Zoch, A., O'Carroll, D. & Zamore, P. D. PIWI-interacting
423 RNAs: small RNAs with big functions. *Nat Rev Genet* **20**, 89-108 (2019).
424 https://doi.org:10.1038/s41576-018-0073-3

425 7 Ramat, A. & Simonelig, M. Functions of PIWI Proteins in Gene Regulation: New Arrows
426 Added to the piRNA Quiver. *Trends Genet* **37**, 188-200 (2021).
427 https://doi.org:10.1016/j.tig.2020.08.011

428 8 Billi, A. C., Fischer, S. E. & Kim, J. K. Endogenous RNAi pathways in C. elegans.
429 *WormBook*, 1-49 (2014). https://doi.org:10.1895/wormbook.1.170.1

430 9 Rojas-Rios, P. & Simonelig, M. piRNAs and PIWI proteins: regulators of gene expression
431 in development and stem cells. *Development* **145** (2018).
432 https://doi.org:10.1242/dev.161786

433 10 Jouravleva, K. & Zamore, P. D. A guide to the biogenesis and functions of endogenous
434 small non-coding RNAs in animals. *Nat Rev Mol Cell Biol* **26**, 347-370 (2025).
435 https://doi.org:10.1038/s41580-024-00818-9
436 11 de Albuquerque, B. F., Placentino, M. & Ketting, R. F. Maternal piRNAs Are Essential for
437 Germline Development following De Novo Establishment of Endo-siRNAs in
438 Caenorhabditis elegans. *Dev Cell* **34**, 448-456 (2015).
439 https://doi.org:10.1016/j.devcel.2015.07.010
440 12 Ramakrishna, N. B. & Miska, E. A. Who watches the watchmen? RNAi pathway-derived
441 ribosomal small RNAs burgeon in absence of piRNAs. *Dev Cell* **56**, 2269-2270 (2021).
442 https://doi.org:10.1016/j.devcel.2021.08.002
443 13 Ortega, J. *et al.* Pachytene piRNAs control discrete meiotic events during
444 spermatogenesis and restrict gene expression in space and time. *Sci Adv* **10**, eadp0466
445 (2024). https://doi.org:10.1126/sciadv.adp0466
446 14 Quarato, P. *et al.* Germline inherited small RNAs facilitate the clearance of untranslated
447 maternal mRNAs in C. elegans embryos. *Nat Commun* **12**, 1441 (2021).
448 https://doi.org:10.1038/s41467-021-21691-6
449 15 Konstantinidou, P. *et al.* A comparative roadmap of PIWI-interacting RNAs across seven
450 species reveals insights into de novo piRNA-precursor formation in mammals. *Cell Rep*
451 **43**, 114777 (2024). https://doi.org:10.1016/j.celrep.2024.114777
452 16 Batista, P. J. *et al.* PRG-1 and 21U-RNAs interact to form the piRNA complex required
453 for fertility in C. elegans. *Mol Cell* **31**, 67-78 (2008).
454 https://doi.org:10.1016/j.molcel.2008.06.002
455 17 Zhang, D. *et al.* The piRNA targeting rules and the resistance to piRNA silencing in
456 endogenous genes. *Science* **359**, 587-592 (2018).
457 https://doi.org:10.1126/science.aao2840

458 18 Bagijn, M. P. *et al.* Function, targets, and evolution of Caenorhabditis elegans piRNAs.
459 *Science* **337**, 574-578 (2012). https://doi.org:10.1126/science.1220952
460 19 Das, P. P. *et al.* Piwi and piRNAs act upstream of an endogenous siRNA pathway to
461 suppress Tc3 transposon mobility in the Caenorhabditis elegans germline. *Mol Cell* **31**,
462 79-90 (2008). https://doi.org:10.1016/j.molcel.2008.06.003
463 20 Gu, W. *et al.* Distinct argonaute-mediated 22G-RNA pathways direct genome
464 surveillance in the C. elegans germline. *Mol Cell* **36**, 231-244 (2009).
465 https://doi.org:10.1016/j.molcel.2009.09.020
466 21 Tu, S. *et al.* Comparative functional characterization of the CSR-1 22G-RNA pathway in
467 Caenorhabditis nematodes. *Nucleic Acids Res* **43**, 208-224 (2015).
468 https://doi.org:10.1093/nar/gku1308
469 22 Singh, M. *et al.* Translation and codon usage regulate Argonaute slicer activity to trigger
470 small RNA biogenesis. *Nat Commun* **12**, 3492 (2021). https://doi.org:10.1038/s41467-
471 021-23615-w
472 23 Vihervaara, A., Duarte, F. M. & Lis, J. T. Molecular mechanisms driving transcriptional
473 stress responses. *Nat Rev Genet* **19**, 385-397 (2018). https://doi.org:10.1038/s41576-
474 018-0001-6
475 24 Gomez-Pastor, R., Burchfiel, E. T. & Thiele, D. J. Regulation of heat shock transcription
476 factors and their roles in physiology and disease. *Nat Rev Mol Cell Biol* **19**, 4-19 (2018).
477 https://doi.org:10.1038/nrm.2017.73
478 25 Lindquist, S. The heat-shock response. *Annu Rev Biochem* **55**, 1151-1191 (1986).
479 https://doi.org:10.1146/annurev.bi.55.070186.005443
480 26 Das, S., Min, S. & Prahlad, V. Gene bookmarking by the heat shock transcription factor
481 programs the insulin-like signaling pathway. *Mol Cell* **81**, 4843-4860 e4848 (2021).
482 https://doi.org:10.1016/j.molcel.2021.09.022

483 27 Weick, E. M. *et al.* PRDE-1 is a nuclear factor essential for the biogenesis of Ruby motif-
484 dependent piRNAs in C. elegans. *Genes Dev* **28**, 783-796 (2014).
485 https://doi.org:10.1101/gad.238105.114
486 28 Weng, C. *et al.* The USTC co-opts an ancient machinery to drive piRNA transcription in
487 C. elegans. *Genes Dev* **33**, 90-102 (2019). https://doi.org:10.1101/gad.319293.118
488 29 Phillips, C. M. & Updike, D. L. Germ granules and gene regulation in the Caenorhabditis
489 elegans germline. *Genetics* **220** (2022). https://doi.org:10.1093/genetics/iyab195
490 30 Ghildiyal, M. & Zamore, P. D. Small silencing RNAs: an expanding universe. *Nat Rev*
491 *Genet* **10**, 94-108 (2009). https://doi.org:10.1038/nrg2504
492 31 Hajdu-Cronin, Y. M., Chen, W. J. & Sternberg, P. W. The L-type cyclin CYL-1 and the
493 heat-shock-factor HSF-1 are required for heat-shock-induced protein expression in
494 Caenorhabditis elegans. *Genetics* **168**, 1937-1949 (2004).
495 https://doi.org:10.1534/genetics.104.028423
496 32 Tate, A. J., Brown, K. C. & Montgomery, T. A. tiny-count: a counting tool for hierarchical
497 classification and quantification of small RNA-seq reads with single-nucleotide precision.
498 *Bioinform Adv* **3**, vbad065 (2023). https://doi.org:10.1093/bioadv/vbad065
499 33 Das, S. *et al.* Serotonin signaling by maternal neurons upon stress ensures progeny
500 survival. *Elife* **9** (2020). https://doi.org:10.7554/eLife.55246
501 34 Jao, C. Y. & Salic, A. Exploring RNA transcription and turnover in vivo by using click
502 chemistry. *Proc Natl Acad Sci U S A* **105**, 15779-15784 (2008).
503 https://doi.org:10.1073/pnas.0808480105
504 35 Rabani, M. *et al.* Metabolic labeling of RNA uncovers principles of RNA production and
505 degradation dynamics in mammalian cells. *Nat Biotechnol* **29**, 436-442 (2011).
506 https://doi.org:10.1038/nbt.1861

507 36 Shalgi, R., Hurt, J. A., Lindquist, S. & Burge, C. B. Widespread inhibition of
508 posttranscriptional splicing shapes the cellular transcriptome following heat shock. *Cell*
509 *Rep* **7**, 1362-1370 (2014). https://doi.org:10.1016/j.celrep.2014.04.044
510 37 Yost, H. J. & Lindquist, S. RNA splicing is interrupted by heat shock and is rescued by
511 heat shock protein synthesis. *Cell* **45**, 185-193 (1986). https://doi.org:10.1016/0092-
512 8674(86)90382-x
513 38 Yost, H. J. & Lindquist, S. Heat shock proteins affect RNA processing during the heat
514 shock response of Saccharomyces cerevisiae. *Mol Cell Biol* **11**, 1062-1068 (1991).
515 https://doi.org:10.1128/mcb.11.2.1062-1068.1991
516 39 Choquet, K., Patop, I. L. & Churchman, L. S. The regulation and function of post-
517 transcriptional RNA splicing. *Nat Rev Genet* **26**, 378-394 (2025).
518 https://doi.org:10.1038/s41576-025-00836-z
519 40 Cote, A. *et al.* Post-transcriptional splicing can occur in a slow-moving zone around the
520 gene. *Elife* **12** (2024). https://doi.org:10.7554/eLife.91357
521 41 Mauger, O., Lemoine, F. & Scheiffele, P. Targeted Intron Retention and Excision for
522 Rapid Gene Regulation in Response to Neuronal Activity. *Neuron* **92**, 1266-1278 (2016).
523 https://doi.org:10.1016/j.neuron.2016.11.032
524 42 Galante, P. A., Sakabe, N. J., Kirschbaum-Slager, N. & de Souza, S. J. Detection and
525 evaluation of intron retention events in the human transcriptome. *RNA* **10**, 757-765
526 (2004). https://doi.org:10.1261/rna.5123504
527 43 Trincado, J. L. *et al.* SUPPA2: fast, accurate, and uncertainty-aware differential splicing
528 analysis across multiple conditions. *Genome Biol* **19**, 40 (2018).
529 https://doi.org:10.1186/s13059-018-1417-1
530 44 Alamancos, G. P., Pages, A., Trincado, J. L., Bellora, N. & Eyras, E. Leveraging
531 transcript quantification for fast computation of alternative splicing profiles. *RNA* **21**,
532 1521-1531 (2015). https://doi.org:10.1261/rna.051557.115

533 45 Wright, C. J., Smith, C. W. J. & Jiggins, C. D. Alternative splicing as a source of
534 phenotypic diversity. *Nat Rev Genet* **23**, 697-710 (2022). https://doi.org:10.1038/s41576-
535 022-00514-4
536 46 Weinreb, A. *et al.* Alternative splicing across the C. elegans nervous system. *Nat*
537 *Commun* **16**, 4508 (2025). https://doi.org:10.1038/s41467-025-58293-5
538 47 Frolows, N. & Ashe, A. Small RNAs and chromatin in the multigenerational epigenetic
539 landscape of Caenorhabditis elegans. *Philos Trans R Soc Lond B Biol Sci* **376**,
540 20200112 (2021). https://doi.org:10.1098/rstb.2020.0112
541 48 Merens, H. E., Choquet, K., Baxter-Koenigs, A. R. & Churchman, L. S. Timing is
542 everything: advances in quantifying splicing kinetics. *Trends Cell Biol* **34**, 968-981
543 (2024). https://doi.org:10.1016/j.tcb.2024.03.007
544 49 Ietswaart, R. *et al.* Genome-wide quantification of RNA flow across subcellular
545 compartments reveals determinants of the mammalian transcript life cycle. *Mol Cell* **84**,
546 2765-2784 e2716 (2024). https://doi.org:10.1016/j.molcel.2024.06.008
547 50 Berg, M. G. *et al.* U1 snRNP determines mRNA length and regulates isoform expression.
548 *Cell* **150**, 53-64 (2012). https://doi.org:10.1016/j.cell.2012.05.029
549 51 Venters, C. C., Oh, J. M., Di, C., So, B. R. & Dreyfuss, G. U1 snRNP Telescripting:
550 Suppression of Premature Transcription Termination in Introns as a New Layer of Gene
551 Regulation. *Cold Spring Harb Perspect Biol* **11** (2019).
552 https://doi.org:10.1101/cshperspect.a032235
553 52 Oh, J. M. *et al.* U1 snRNP telescripting regulates a size-function-stratified human
554 genome. *Nat Struct Mol Biol* **24**, 993-999 (2017). https://doi.org:10.1038/nsmb.3473
555 53 Cugusi, S. *et al.* Heat shock induces premature transcript termination and reconfigures
556 the human transcriptome. *Mol Cell* **82**, 1573-1588 e1510 (2022).
557 https://doi.org:10.1016/j.molcel.2022.01.007

558 54 Peng, A. Y. T. & Freeman, B. C. Inhibiting U1 telescripting: A means to an end for
559 transcription. *Mol Cell* **82**, 1405-1407 (2022).
560 https://doi.org:10.1016/j.molcel.2022.04.001
561 55 Lau, B. T. & Ji, H. P. Single molecule counting and assessment of random molecular
562 tagging errors with transposable giga-scale error-correcting barcodes. *BMC Genomics*
563 **18**, 745 (2017). https://doi.org:10.1186/s12864-017-4141-4
564 56 Tsagiopoulou, M. *et al.* UMIc: A Preprocessing Method for UMI Deduplication and Reads
565 Correction. *Front Genet* **12**, 660366 (2021). https://doi.org:10.3389/fgene.2021.660366
566 57 Smith, T., Heger, A. & Sudbery, I. UMI-tools: modeling sequencing errors in Unique
567 Molecular Identifiers to improve quantification accuracy. *Genome Res* **27**, 491-499
568 (2017). https://doi.org:10.1101/gr.209601.116
569 58 Lebrigand, K., Magnone, V., Barbry, P. & Waldmann, R. High throughput error corrected
570 Nanopore single cell transcriptome sequencing. *Nat Commun* **11**, 4025 (2020).
571 https://doi.org:10.1038/s41467-020-17800-6
572 59 Reid-Bayliss, K. S. & Loeb, L. A. Accurate RNA consensus sequencing for high-fidelity
573 detection of transcriptional mutagenesis-induced epimutations. *Proc Natl Acad Sci U S A*
574 **114**, 9415-9420 (2017). https://doi.org:10.1073/pnas.1709166114
575 60 Thomas, M. J., Platas, A. A. & Hawley, D. K. Transcriptional fidelity and proofreading by
576 RNA polymerase II. *Cell* **93**, 627-637 (1998). https://doi.org:10.1016/s0092-
577 8674(00)81191-5
578 61 Hwang, J. & Maquat, L. E. Nonsense-mediated mRNA decay (NMD) in animal
579 embryogenesis: to die or not to die, that is the question. *Curr Opin Genet Dev* **21**, 422-
580 430 (2011). https://doi.org:10.1016/j.gde.2011.03.008
581 62 Kurosaki, T., Popp, M. W. & Maquat, L. E. Quality and quantity control of gene
582 expression by nonsense-mediated mRNA decay. *Nat Rev Mol Cell Biol* **20**, 406-420
583 (2019). https://doi.org:10.1038/s41580-019-0126-2

584 63 Maquat, L. E. Nonsense-mediated mRNA decay: splicing, translation and mRNP
585 dynamics. *Nat Rev Mol Cell Biol* **5**, 89-99 (2004). https://doi.org:10.1038/nrm1310
586 64 Johns, L., Grimson, A., Kuchma, S. L., Newman, C. L. & Anderson, P. Caenorhabditis
587 elegans SMG-2 selectively marks mRNAs containing premature translation termination
588 codons. *Mol Cell Biol* **27**, 5630-5638 (2007). https://doi.org:10.1128/MCB.00410-07
589 65 Mitrovich, Q. M. & Anderson, P. mRNA surveillance of expressed pseudogenes in C.
590 elegans. *Curr Biol* **15**, 963-967 (2005). https://doi.org:10.1016/j.cub.2005.04.055
591 66 Muir, V. S., Gasch, A. P. & Anderson, P. The Substrates of Nonsense-Mediated mRNA
592 Decay in Caenorhabditis elegans. *G3 (Bethesda)* **8**, 195-205 (2018).
593 https://doi.org:10.1534/g3.117.300254
594 67 Pulak, R. & Anderson, P. mRNA surveillance by the Caenorhabditis elegans smg genes.
595 *Genes Dev* **7**, 1885-1897 (1993). https://doi.org:10.1101/gad.7.10.1885
596 68 Hodgkin, J., Papp, A., Pulak, R., Ambros, V. & Anderson, P. A new kind of informational
597 suppression in the nematode Caenorhabditis elegans. *Genetics* **123**, 301-313 (1989).
598 https://doi.org:10.1093/genetics/123.2.301
599 69 Watanabe, T. & Lin, H. Posttranscriptional regulation of gene expression by Piwi proteins
600 and piRNAs. *Mol Cell* **56**, 18-27 (2014). https://doi.org:10.1016/j.molcel.2014.09.012
601 70 Wang, X., Ramat, A., Simonelig, M. & Liu, M. F. Emerging roles and functional
602 mechanisms of PIWI-interacting RNAs. *Nat Rev Mol Cell Biol* **24**, 123-141 (2023).
603 https://doi.org:10.1038/s41580-022-00528-0
604 71 Teixeira, F. K. *et al.* piRNA-mediated regulation of transposon alternative splicing in the
605 soma and germ line. *Nature* **552**, 268-272 (2017). https://doi.org:10.1038/nature25018
606 72 He, J. *et al.* piRNA-guided intron removal from pre-mRNAs regulates density-dependent
607 reproductive strategy. *Cell Rep* **39**, 110593 (2022).
608 https://doi.org:10.1016/j.celrep.2022.110593

609 73 Akay, A. *et al.* The Helicase Aquarius/EMB-4 Is Required to Overcome Intronic Barriers
610 to Allow Nuclear RNAi Pathways to Heritably Silence Transcription. *Dev Cell* **42**, 241-255
611 e246 (2017). https://doi.org:10.1016/j.devcel.2017.07.002
612 74 Tyc, K. M. *et al.* The Conserved Intron Binding Protein EMB-4 Plays Differential Roles in
613 Germline Small RNA Pathways of C. elegans. *Dev Cell* **42**, 256-270 e256 (2017).
614 https://doi.org:10.1016/j.devcel.2017.07.003
615 75 Makeyeva, Y. V., Shirayama, M. & Mello, C. C. Cues from mRNA splicing prevent default
616 Argonaute silencing in C. elegans. *Dev Cell* **56**, 2636-2648 e2634 (2021).
617 https://doi.org:10.1016/j.devcel.2021.08.022
618 76 Hutcheon, K. *et al.* Analysis of the small non-protein-coding RNA profile of mouse
619 spermatozoa reveals specific enrichment of piRNAs within mature spermatozoa. *RNA*
620 *Biol* **14**, 1776-1790 (2017). https://doi.org:10.1080/15476286.2017.1356569
621 77 Simon, M. *et al.* Reduced insulin/IGF-1 signaling restores germ cell immortality to
622 Caenorhabditis elegans Piwi mutants. *Cell Rep* **7**, 762-773 (2014).
623 https://doi.org:10.1016/j.celrep.2014.03.056
624 78 Son, H. G. *et al.* RNA surveillance via nonsense-mediated mRNA decay is crucial for
625 longevity in daf-2/insulin/IGF-1 mutant C. elegans. *Nat Commun* **8**, 14749 (2017).
626 https://doi.org:10.1038/ncomms14749
627 79 Kim, E. J. E. *et al.* Caenorhabditis elegans algn-2 Is Critical for Longevity Conferred by
628 Enhanced Nonsense-Mediated mRNA Decay. *iScience* **23**, 101713 (2020).
629 https://doi.org:10.1016/j.isci.2020.101713
630 80 Dumesic, P. A. & Madhani, H. D. The spliceosome as a transposon sensor. *RNA Biol* **10**,
631 1653-1660 (2013). https://doi.org:10.4161/rna.26800
632

Figure 1

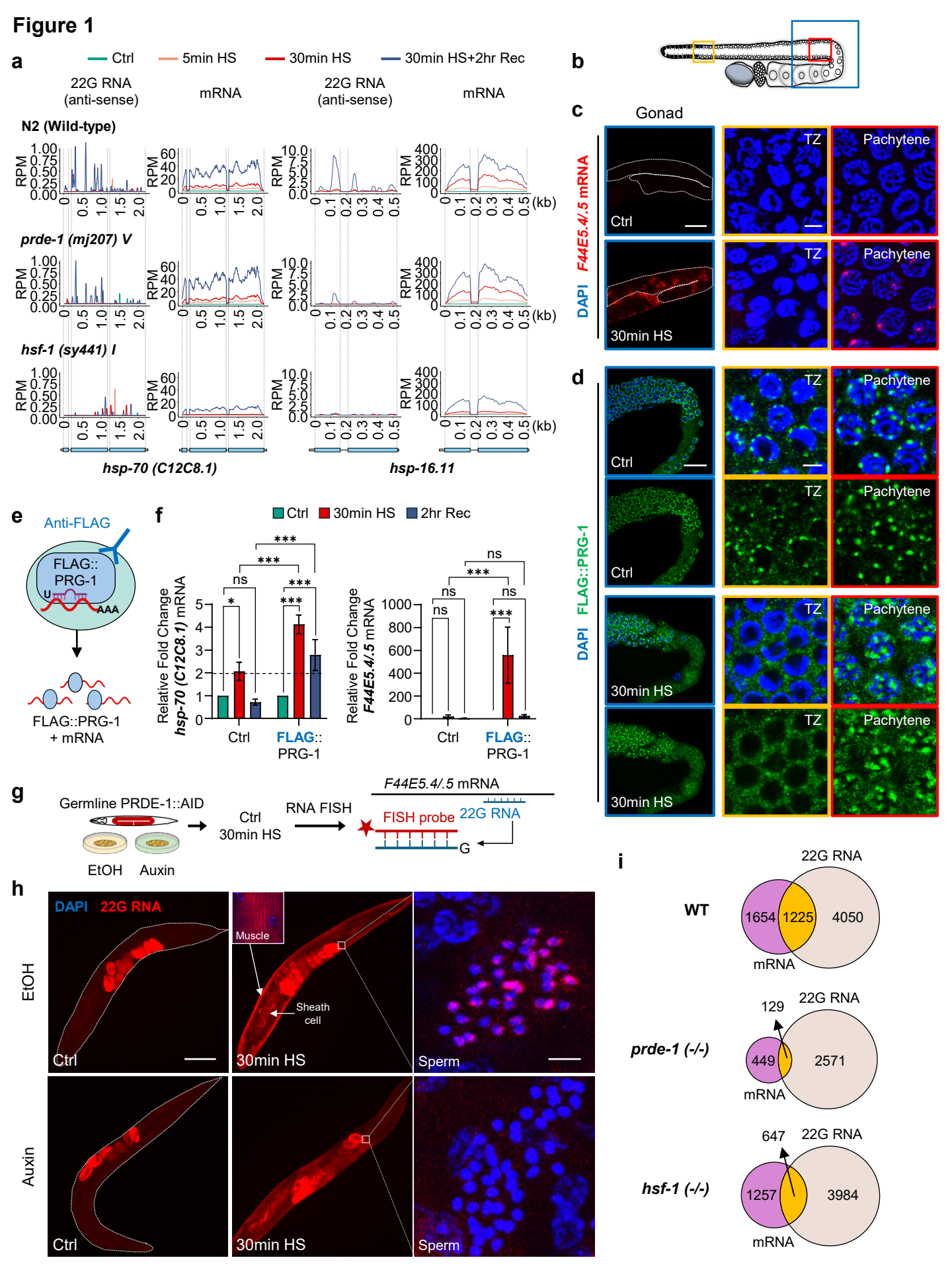
a
Ctrl
5min HS
30min HS
30min HS+2hr Rec
22G RNA (anti-sense)
mRNA
22G RNA (anti-sense)
mRNA
N2 (Wild-type)
prde-1 (mj207) V
hsf-1 (sy441) I
RPM
(kb)
hsp-70 (C12C8.1)
hsp-16.11
b
c
Gonad
F44E5.4/.5 mRNA
DAPI
Ctrl
30min HS
TZ
Pachytene
d
FLAG::PRG-1
DAPI
Ctrl
30min HS
TZ
Pachytene
e
Anti-FLAG
FLAG:: PRG-1
U
AAA
FLAG::PRG-1 + mRNA
f
Ctrl
30min HS
2hr Rec
Relative Fold Change hsp-70 (C12C8.1) mRNA
Relative Fold Change F44E5.4/.5 mRNA
ns
*
***
Ctrl
FLAG:: PRG-1
g
Germline PRDE-1::AID
EtOH
Auxin
Ctrl
30min HS
RNA FISH
F44E5.4/.5 mRNA
FISH probe
22G RNA
G
h
DAPI
22G RNA
EtOH
Auxin
Muscle
Sheath cell
Ctrl
30min HS
Sperm
i
WT
22G RNA
mRNA
1654
1225
4050
prde-1 (-/-)
129
449
2571
hsf-1 (-/-)
647
1257
3984

Figure 1. Piwi-interacting RNAs (piRNAs) target *hsp* mRNAs upon heat shock.

a. Metaprofile plots showing normalized antisense 22G-RNA reads (RPM), and mRNA reads (RPM) across *hsp* mRNAs in wild-type (WT, *C. elegans* wild isolate, var Bristol), *prde-1(mj207) V,* and *hsf-1(sy441) I* mutants. **Top**: conditions of heat shock. **Bottom**: Schematic of *hsp* genes analyzed.

b-d. Spatial localization of *hsp-70* mRNA and PIWI (PRG-1) in the WT germlines. **(b)** Schematic of gonad regions in **c** and **d**: Blue box, Gonad region shown. Orange box, transition zone (TZ). Red box, Late pachytene. Representative confocal images of each region showing **(c)** *hsp-70 (F44E5.4/.5)* mRNA localized using RNA Fluorescence *in situ* hybridization (RNA FISH; Projected image), and **(d)** PIWI (FLAG::PRG-1) by immunostaining with anti-FLAG antibody (Z-section). Germlines from non-heat-shocked (Ctrl) and heat-shock-exposed (30min HS) animals are shown. Red: *hsp-70 (F44E5.4/.5)* mRNA. Green: FLAG::PRG-1. Blue: DNA staining with DAPI. Scale bars, c: 50 μm (Gonad), and 3 μm (TZ, Pachytene). Scale bars, d: 20 μm (Gonad), and 3 μm (TZ, Pachytene).

e, f. Native RNA immunoprecipitation (RIP) to probe *hsp* mRNA's association with PIWI (FLAG::PRG-1). **(e)** Experiment Schematic. **(f)** Relative fold change (RT-qPCR) in *hsp-70s* (*C12C8.1* and *F44E5.4/.5*) mRNAs that immunoprecipitated with PIWI. *hsp* mRNA levels were normalized to *pmp*-3 (input) and are shown relative to non-heat-shocked animals. Ctrl: wild-type animals with no FLAG-tagged proteins were negative controls. *bath-45* served as positive control (Suppl. Fig 2b). Legend: Treatment conditions. Bars: mean value. Error bars: standard error. n = 3-5 biologically independent experiments. Statistical analysis: 2-way ANOVA.

g, h. Germline depletion of PRDE-1 using the auxin-inducible degron (AID) system followed by RNA FISH to detect 22G-RNAs antisense to *hsp-70 (F44E5.4/.5).* **(g)** Experiment schematic: EtOH: Vehicle control. Probe design shown. **(h)** Representative micrographs (projected confocal Z-sections) showing RNA FISH of 22G-RNA under control conditions (EtOH) and upon PRDE-1 depletion (auxin). Red: 22G-RNA. Blue: DAPI stained DNA. Expression in muscle (arrow, box) and gonad sheath cells (arrow), and in sperm (highlighted). Embryos staining is non-specific. Scale bars: 100 μm (Ctrl, 30min HS), and 3 μm (Sperm).

i. Venn diagrams showing overlap between differentially expressed mRNAs and 22G-RNAs upon 30 minutes heat shock in WT, *prde-1* and *hsf-1* mutants.

Figure 2

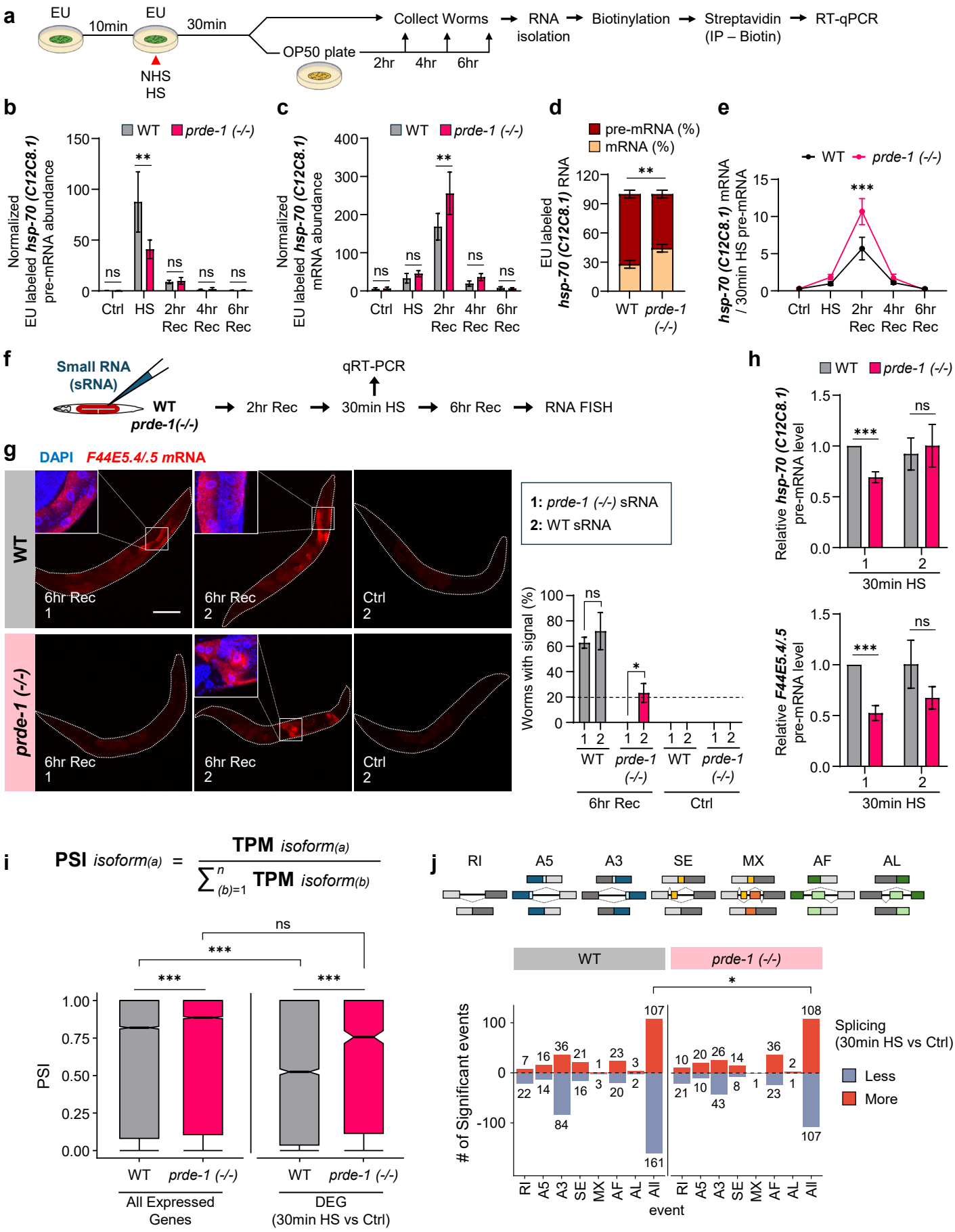
a
EU
10min
EU
30min
NHS
HS
OP50 plate
2hr
4hr
6hr
Collect Worms
RNA isolation
Biotinylation
Streptavidin (IP – Biotin)
RT-qPCR
b
WT
prde-1 (-/-)
Normalized EU labeled hsp-70 (C12C8.1) pre-mRNA abundance
Ctrl
HS
2hr Rec
4hr Rec
6hr Rec
c
Normalized EU labeled hsp-70 (C12C8.1) mRNA abundance
d
pre-mRNA (%)
mRNA (%)
EU labeled hsp-70 (C12C8.1) RNA
e
hsp-70 (C12C8.1) mRNA / 30min HS pre-mRNA
f
Small RNA (sRNA)
WT
prde-1(-/-)
2hr Rec
qRT-PCR
30min HS
6hr Rec
RNA FISH
g
DAPI
F44E5.4/.5 mRNA
6hr Rec 1
6hr Rec 2
Ctrl 2
1: prde-1 (-/-) sRNA
2: WT sRNA
Worms with signal (%)
6hr Rec
Ctrl
h
Relative hsp-70 (C12C8.1) pre-mRNA level
Relative F44E5.4/.5 pre-mRNA level
30min HS
i
PSI isoform(a) = TPM isoform(a) / Σ(b)=1 n TPM isoform(b)
PSI
All Expressed Genes
DEG (30min HS vs Ctrl)
j
RI
A5
A3
SE
MX
AF
AL
# of Significant events
event
All
Splicing (30min HS vs Ctrl)
Less
More

Figure 2. piRNAs delay *hsp* mRNAs splicing.

a-e. Metabolic pulse-chase labeling with EU and quantification of *hsp* RNA. **(a)** Experiment schematic: animals were fed EU-mixed bacteria 10 minutes before heat shock (pre-loading), heat shocked for 30 minutes (pulse-labeling nascent RNA), and moved onto unlabeled bacterial plates (chase). The EU-labeled nascent RNA was isolated from NHS animals (Ctrl), heat-shocked animals immediately after 30 min heat-shock (HS), and after 2,4, and 6 hrs post-heat shock recovery (Rec), biotin-conjugated, and immunoprecipitated. Normalized absolute RNA abundance was quantified by RT-qPCR (see methods; *pmp-3* mRNA used to normalize for variability in labeling). EU-labeled *hsp-70 (C12C8.1)* **(b)** pre-mRNA and **(c)** mRNA abundance. Y-axis: Normalized abundance. X-axis: Treatments. Note EU-labeled mRNA is derived from the splicing of EU-labeled pre-mRNA. **(d)** Percentages of pre-mRNA and mRNA in total EU-labeled RNA after 30 min heat shock. **(e)** Relative amounts of EU-labeled spliced mRNAs produced from the nascent EU-labeled unspliced pre-mRNA. Values normalized to *pmp-3*. Y-axis: Relative abundance. X-axis: Treatment. Bars (b-d) and line graph (e): mean value. Error bars: standard error. (b, c, e) n = 5~13 biologically independent experiments. Statistical analysis: 2 way-ANOVA; (d) n = 14 biologically independent experiments. Statistical analysis: two-tailed unpaired t-test.

f, g. Microinjection of small RNA fractions isolated from WT animals rescues *hsp*-70 fate. **(f)** Experiment schematic: small RNA fractions purified from heat-shocked WT and *prde-1* animals were injected into WT and *prde-1* animals shortly before heat-shock exposure, and animals were probed for *hsp-70 (F44E5.4/.5)* 6 hours post-heat shock. Non-heat-shock animals were injected to control for effects of injection alone. **(g)** RNA FISH of *hsp-70 (F44E5.4/.5)* in WT and *prde-1* animals 6 hours following heat shock or under NHS conditions. Injection mix (box) and treatment indicated. Red: *hsp-70 (F544E5.4/.5)* mRNA. Blue: DNA staining with DAPI. Scale

bars: 100 µm. **Right:** Quantification of results. Y-axis: Percentage of injected animals positive for *hsp-70*. X-axis: Injection mix, strains and treatment. Bars: mean value. Error bars: standard error. n = 17~22 worms (6hr Rec), 6~10 worms (Ctrl). Statistical analysis: Fisher's exact test.

h. Microinjection of small RNA fractions isolated from heat-shocked WT animals rescues *hsp*-70 pre-mRNA levels. Normalized RT-qPCR of relative fold change of *hsp-70s* (*C12C8.1 and F44E5.4/.5*) pre-mRNAs following sRNA injection. Y-axis: *hsp-70* pre-mRNA levels, normalized to *pmp-3*, relative to heat-shocked wild-type animals injected with small RNAs from *prde-1* mutants. X-axis: Injection mix (see box in Fig 2g). Bars: mean value. Error bars: standard error. n = 6 biologically independent experiments. Statistical analysis: two-tailed unpaired t-test.

i. Genes differentially regulated by heat shock in WT, but not *prde-1* animals, are enriched for alternative spliced isoforms. **Top**: Calculation of PSI "percent spliced in" values. **Bottom**: Alternative spliced isoforms, as reflected by PSI values, in all expressed genes, and in differentially expressed genes (p.adj <0.05) in wild-type and *prde-1* animals. Boxplots: median value depicted. Error bars: standard error. Statistical analysis: two-tailed unpaired t-test.

j. Alternative splicing (AS) events in WT and *prde-1* animals upon heat shock. **Top**: AS events, retained intron (RI), alternative 5'/3' Splice Sites (A5/A3), skipped exon (SE), mutually exclusive exons (MX), and alternative first and last exons (AF/AL). **Bottom**: Number of AS events amongst differentially expressed genes (HS vs NHS condition; p.adj <0.05) in WT and *prde-1* mutants. Bars: Number of events (splicing increase or decrease relative to NHS condition). Statistical analysis: Chi-square analysis.

Figure 3

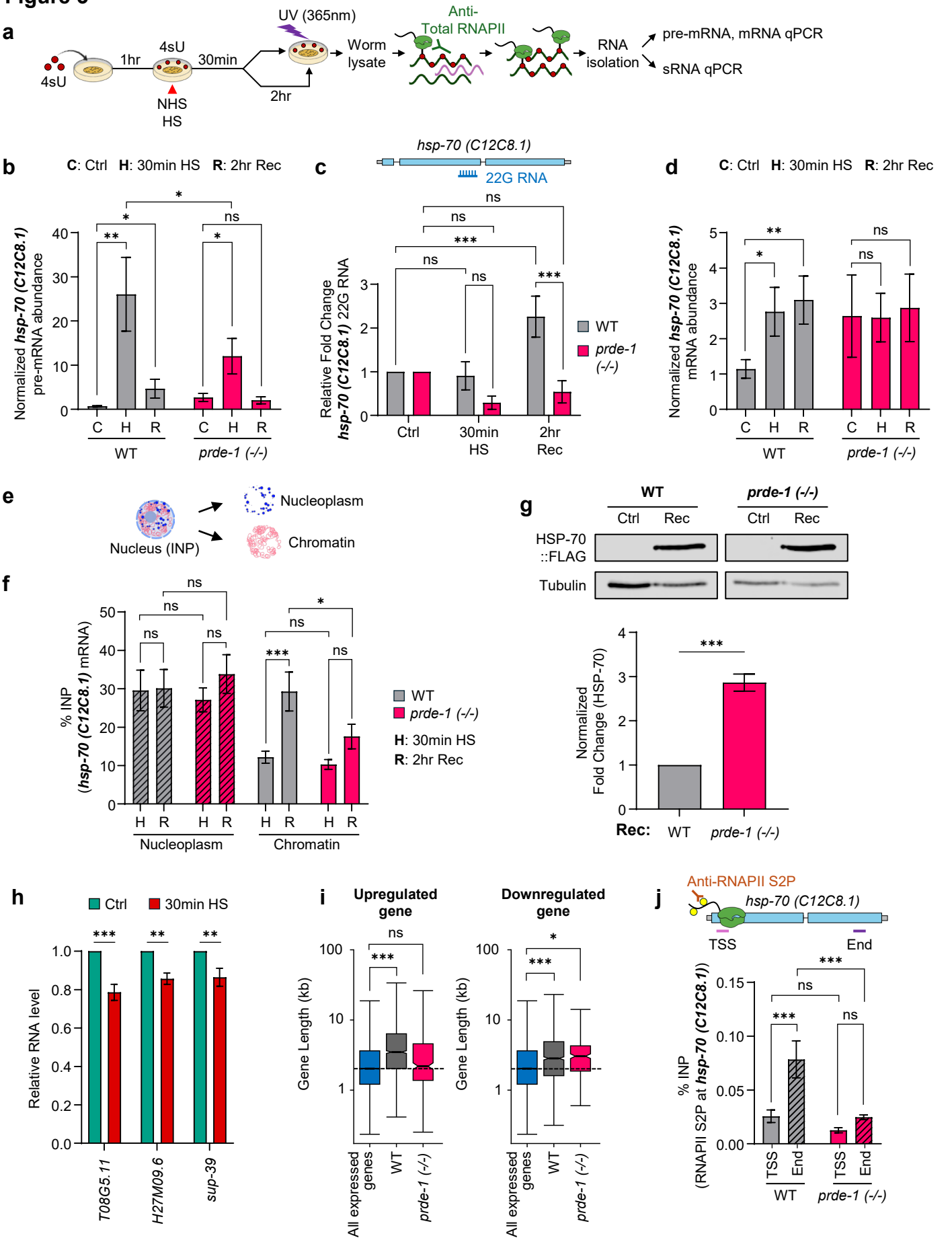
a
4sU
1hr
4sU
NHS
HS
30min
UV (365nm)
2hr
Worm lysate
Anti-Total RNAPII
RNA isolation
pre-mRNA, mRNA qPCR
sRNA qPCR
b
C: Ctrl H: 30min HS R: 2hr Rec
Normalized hsp-70 (C12C8.1) pre-mRNA abundance
WT
prde-1 (-/-)
c
hsp-70 (C12C8.1)
22G RNA
Relative Fold Change hsp-70 (C12C8.1) 22G RNA
Ctrl
30min HS
2hr Rec
WT
prde-1 (-/-)
d
C: Ctrl H: 30min HS R: 2hr Rec
Normalized hsp-70 (C12C8.1) mRNA abundance
WT
prde-1 (-/-)
e
Nucleus (INP)
Nucleoplasm
Chromatin
f
% INP (hsp-70 (C12C8.1) mRNA)
Nucleoplasm
Chromatin
WT
prde-1 (-/-)
H: 30min HS
R: 2hr Rec
g
WT
prde-1 (-/-)
Ctrl
Rec
HSP-70 ::FLAG
Tubulin
Normalized Fold Change (HSP-70)
Rec:
WT
prde-1 (-/-)
h
Ctrl
30min HS
Relative RNA level
T08G5.11
H27M09.6
sup-39
i
Upregulated gene
Downregulated gene
Gene Length (kb)
All expressed genes
WT
prde-1 (-/-)
j
Anti-RNAPII S2P
hsp-70 (C12C8.1)
TSS
End
% INP (RNAPII S2P at hsp-70 (C12C8.1))
WT
prde-1 (-/-)

Figure 3. Antisense 22G-RNAs associated with RNA Polymerase II at the transcription complex to modulate post-transcriptional splicing.

a-d. Modified PAR-CLIP to assess 22G-RNAs' role in splicing. **(a)** Experiment schematic: Animals were fed 4sU-mixed bacteria, subjected to heat shock, exposed to UV (365 nm) either immediately or after 2 hours of recovery, RNA Pol II was immunoprecipitated, *hsp* mRNA and pre-mRNA were quantified by computing absolute RNA abundance (RT-qPCR and standard curves; *pmp-3* mRNA used to normalize for variability in IP amounts across samples and experiments) and 22G-RNA quantified as relative fold change using stem loop PCR (design shown). See Suppl. Fig 7c for details. Amounts of **(b)** *hsp-70 (C12C8.1)* pre-mRNA, **(c)** 22G-RNA, and **(d)** *hsp-70 (C12C8.1)* mRNA that cross-linked to, and immunoprecipitated with Pol II. Y-axis: Normalized or relative abundance. X-axis: Treatment conditions (see top legend). Bars: mean value. Error bars: standard error. (b) n = 8~13 biologically independent experiments. Statistical analysis: two-tailed unpaired t-test (within strain) and 2-way ANOVA (between strains); (c) n = 5~6 biologically independent experiments. Statistical analysis: 2-way ANOVA; (d) n = 5~10 biologically independent experiments. Statistical analysis: 2-way ANOVA.

e, f. Nuclear fractionation to assess chromatin retention of *hsp-70* RNA. **(e)** Experiment schematic. Nuclei were isolated, fractionated to obtain nucleoplasm and chromatin, and enrichment of *hsp-70* mRNA in both fractions was determined. **(f)** Fold enrichment over input (nuclei) of *hsp-70 (C12C8.1)* mRNA in respective fractions. Y-axis: % input (total nucleus). X-axis: Nuclear fraction, strain, and treatment. Bars: mean value. Error bars: standard error. n = 9~10 biologically independent experiments. Statistical analysis: 2-way ANOVA.

g. HSP-70 protein levels in WT and *prde-1.* **Top:** Representative western blot image showing HSP-70(C12C8.1)::FLAG in NHS (Ctrl) or after heat-shock in WT and *prde-1* animals

expressing endogenous *flag*-tagged *hsp-70*. Animals harvested 3 hrs following HS (Rec) to allow HSP-70 protein synthesis. Tubulin: loading control. **Bottom:** Relative HSP-70 protein expression (relative to wild-type heat-shocked levels, because control animals do not express detectable HSP-70 protein). Bars: mean value. Error bars: standard error. n = 3 biologically independent experiments. Statistical analysis: two-tailed unpaired t-test.

h. U1 RNA levels upon heat shock in WT animals (RT-qPCR: relative fold change). U1 RNA values normalized to *pmp-3* mRNA values and shown relative to NHS levels. X-axis: U1 RNAs. Bars: mean value. Error bars: standard error. n = 3~4 biologically independent experiments. Statistical analysis: 2-way ANOVA.

i. Gene length dependence of heat-shock upregulated and downregulated protein-coding genes genes (p.adj <0.05). Y-axis: Average gene lengths (kb). X-axis: Strain. Genome-wide gene lengths of all expressed genes depicted for comparison. Boxplots: median value depicted. Error bars: standard error. Statistical analysis: Tukey HSD.

j. Elongating RNA polymerase II (anti-S2P) levels at *hsp* gene. **Top:** Schematic of *hsp-70 (C12C8.1)* gene, and regions probed: Transcription Start Site (TSS) and distal regions (3') of *hsp-70* (*C12C8.1*). **Bottom:** ChIP-qPCR showing fold enrichment over input. Y-axis: % ChIP input. X-axis: Strain, and region assayed. Bars: mean value. Error bars: standard error. n = 4~8 biologically independent experiments. Statistical analysis: 2-way ANOVA.

Figure 4

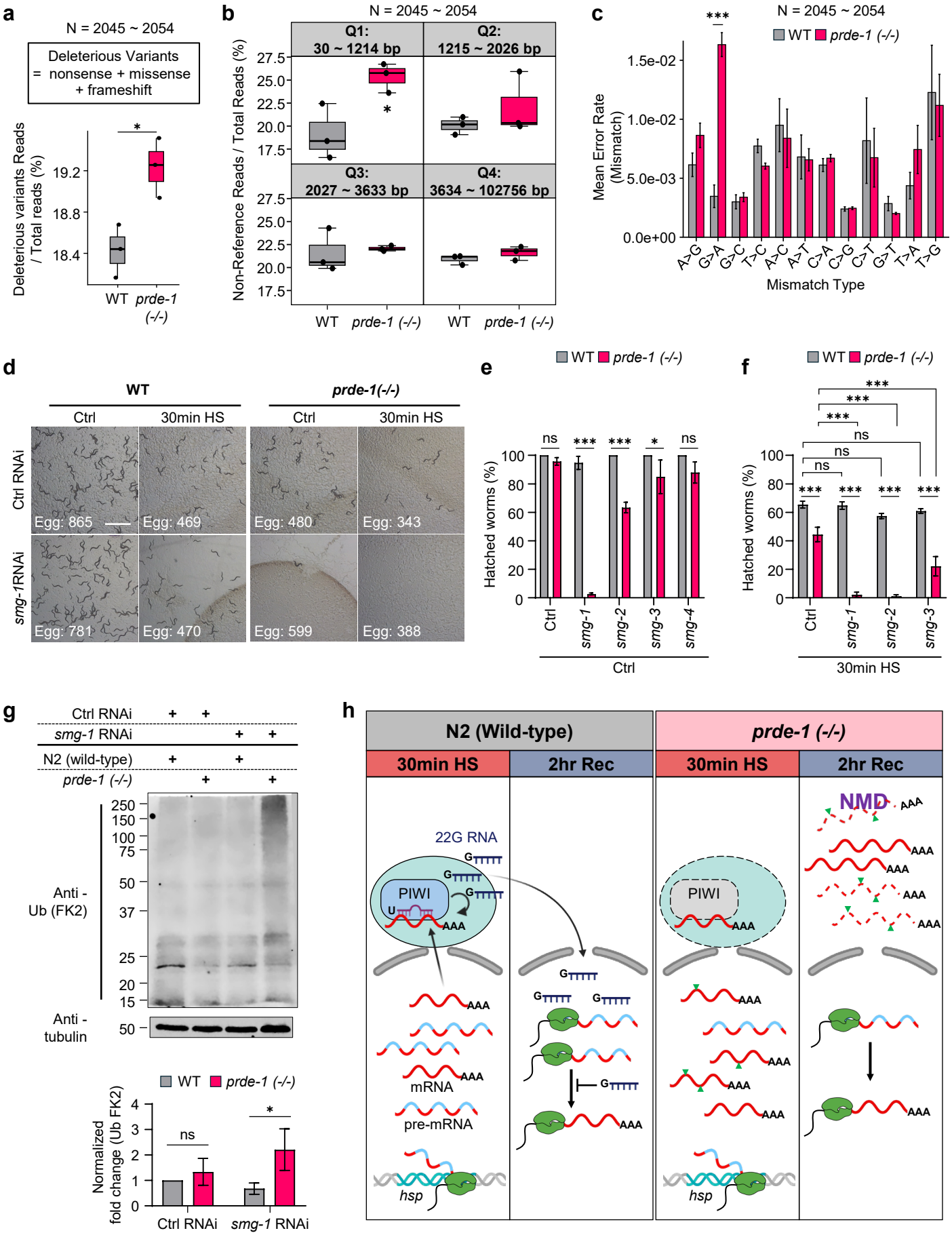
a
N = 2045 ~ 2054
Deleterious Variants = nonsense + missense + frameshift
Deleterious variants Reads / Total reads (%)
WT
prde-1 (-/-)
b
N = 2045 ~ 2054
Q1: 30 ~ 1214 bp
Q2: 1215 ~ 2026 bp
Q3: 2027 ~ 3633 bp
Q4: 3634 ~ 102756 bp
Non-Reference Reads / Total Reads (%)
c
N = 2045 ~ 2054
WT prde-1 (-/-)
Mean Error Rate (Mismatch)
Mismatch Type
d
WT
prde-1(-/-)
Ctrl
30min HS
Ctrl RNAi
smg-1RNAi
Egg: 865
Egg: 469
Egg: 480
Egg: 343
Egg: 781
Egg: 470
Egg: 599
Egg: 388
e
WT prde-1 (-/-)
Hatched worms (%)
Ctrl
smg-1
smg-2
smg-3
smg-4
f
WT prde-1 (-/-)
Hatched worms (%)
30min HS
g
Ctrl RNAi
smg-1 RNAi
N2 (wild-type)
prde-1 (-/-)
Anti - Ub (FK2)
Anti - tubulin
Normalized fold change (Ub FK2)
Ctrl RNAi
smg-1 RNAi
h
N2 (Wild-type)
prde-1 (-/-)
30min HS
2hr Rec
22G RNA
PIWI
mRNA
pre-mRNA
hsp
NMD

Figure 4. piRNA protects transcript fidelity and complements nonsense-mediated decay (NMD) to maintain protein quality control.

a. Percentage of nonsense, missense, and frameshift variants containing mRNA molecules in wild type and *prde-1* mutants (variants identified by GATK and SnpEff). Y-axis: % variants. X-axis: Strain. Total variant containing sites=2045-2054. Approximately 2.7 x 10^7 individual mRNAs analyzed. Boxplots: median value depicted. Error bars: standard error. Statistical analysis: two-tailed unpaired t-test.

b. Gene length stratification of mRNA variants in *prde*-1. Percentage of variants among total variant-containing mRNA molecules expressed from genes of different lengths in wild type and *prde-1* mutants. Q1-Q4: Genome divided into quantiles by gene length, as in Suppl. Fig 8b, c (gene lengths in bp). Y-axis: % variants. X-axis: Strain. Boxplots: median value depicted. Error bars: standard error. Statistical analysis: two-tailed unpaired t-test.

c. Mean mismatch rates amongst variant-containing mRNA molecules. Y-axis: Mean error rate (number of mismatch reads/total reads with variants). X-axis: Mismatch. Total variant containing sites=2045-2054. Approximately 2.7 x 10^7 individual mRNAs analyzed. Bars: mean value. Error bars: standard error. Statistical analysis: two-tailed unpaired t-test.

d-f. Dependence on NMD. **(d)** Representative DIC micrographs of progeny from control and heat-shocked WT and *prde-1* animals on Ctrl (L4440) and *smg-1* RNAi. The number of eggs laid by the mothers in one representative experiment is shown. Note: WT progeny have grown into adults. Scale bar: 2mm. (**e, f**) Percent viable embryos from mothers subjected to RNAi-mediated downregulation of NMD components under **(e)** control, and **(f)** heat shock conditions. Y-axis: Percentage of viable embryos. X-axis: Strain and RNAi-treatment. Bars: mean value. Error bars:

standard error. n = 3~5 biologically independent experiments. Statistical analysis: 2 way-ANOVA.

g. Polyubiquitinated protein levels in WT and *prde*-1animals exposed to control (L4440) or *smg-1* RNAi. **Top:** Representative western blot (antibody:clone FK2). Tubulin: loading control. **Bottom:** Quantification of polyubiquitinated protein (normalized to wild-type Control RNAi-treated animals). Bars: mean value. Error bars: standard error. n = 5 biologically independent experiments. Statistical analysis: 2 way-ANOVA.

h. Model for the mechanism through which piRNA/22G-RNA pathway regulates splicing.

Suppl. Figure 1

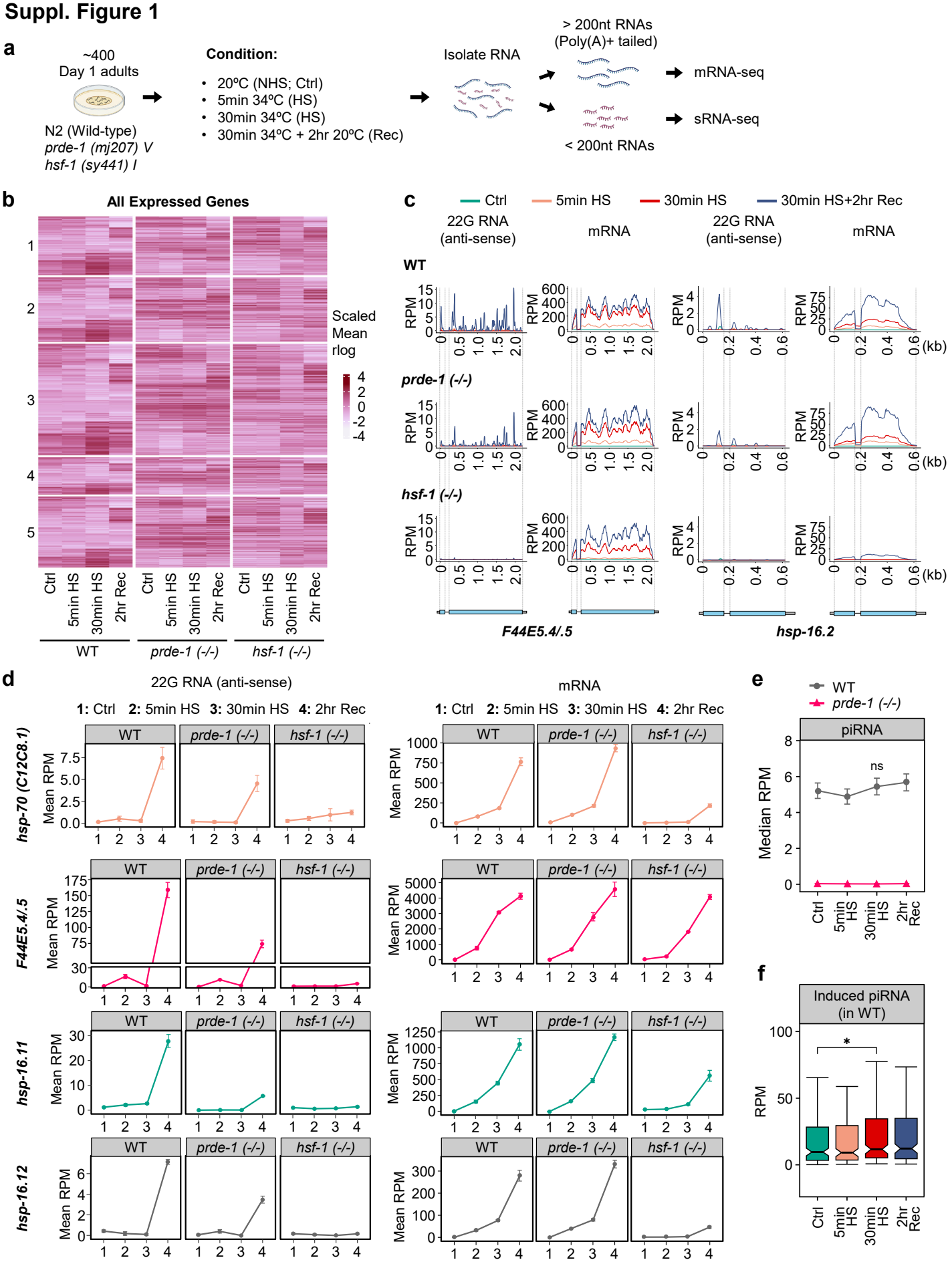

Supplementary Figure 1. Piwi-interacting RNAs (piRNAs) target *hsp* mRNAs upon heat shock.

a. RNA-sequencing experiment schematic.

b. Heatmaps: Wild type (N2; WT, left), *prde-1* (middle), and *hsf-1* (right). Mean expression values of the regularized log (rlog) transformed counts for all expressed genes shown for each strain. Expression scaled row-wise (z-score) to highlight relative changes. K-means clustering was performed on the gene expression of the WT samples, and gene order and clustering (1-5) are preserved across strains and treatments. Columns: treatments [Non heat shocked control (NHS; Ctrl), 5 minutes heat shock (5min HS), 30 minutes heat shock (30min HS), and 2 hours recovery (2hr Rec)]. Color bar: scaled expression level.

c. Metaprofile plots showing normalized antisense 22G-RNA reads (RPM), and mRNA reads (RPM) across *hsp* mRNAs in wild-type (WT), *prde-1* and *hsf-1* mutants. **Top**: Conditions of heat shock. **Bottom**: Schematic of *hsp* genes analyzed.

d. Left: Normalized expression (RPM) of 22G-RNAs antisense to *hsp* genes. **Right:** Normalized expression (PRM) of *hsp* mRNAs in WT, *prde*-1, and *hsf-1* mutants. Y-axis: Expression (RPM). X-axis: Treatments (see top legend).

e. Normalized expression (RPM) of piRNAs in WT and *prde*-1 mutants. RPM >0.5 in at least one sample and RPM >0 in at least replicates were counted. Statistical analysis: Wilcoxon test.

f. Boxplot showing normalized expression (RPM) of significantly differentially expressed piRNAs between the WT 30 minutes heat shock and control conditions. Boxplots: median value depicted. Y-axis: Expression (RPM). X-axis: Treatments. Statistical analysis: Wilcoxon test.

Suppl. Figure 2

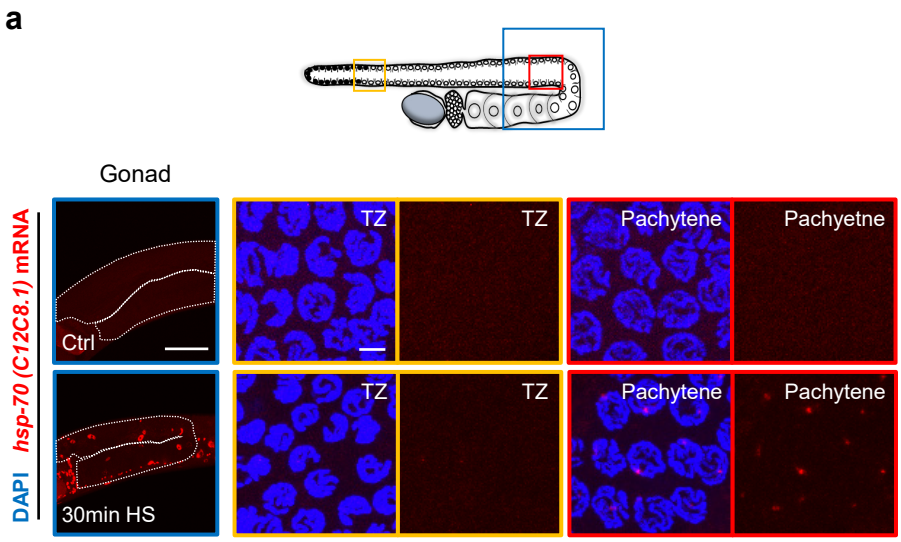

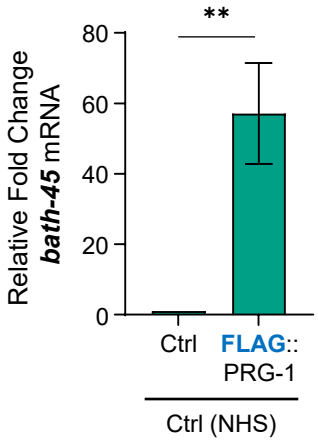

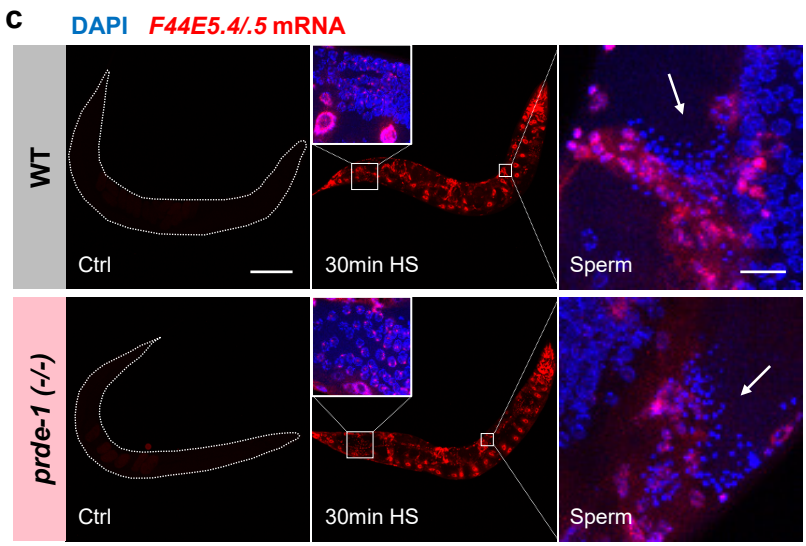

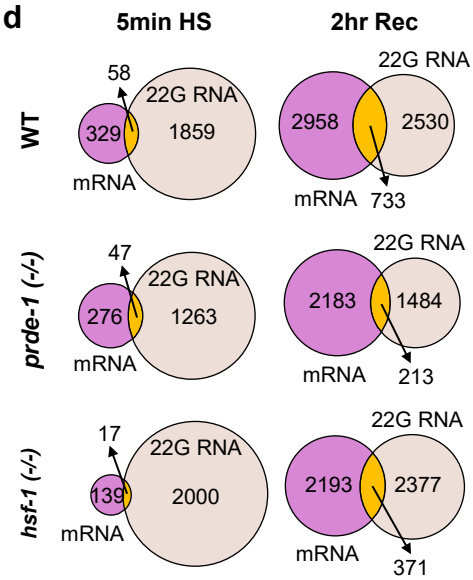

Supplementary Figure 2. piRNAs target *hsp* mRNAs expressed in the germline upon heat shock to generate 22G-RNAs.

a. Representative micrographs of projected confocal Z-sections of regions (Gonad, TZ, and Pachytene) showing RNA Fluorescence *in situ* hybridization (RNA FISH) of *hsp-70 (C12C8.1)* in WT animals. Red: *hsp-70 (C12C8.1)* mRNA. Blue: DNA staining with DAPI. Similar to Fig 1b, c. Scale bars: 50 μm (Gonad) and 3 μm (TZ, Pachytene).

b. *bath-45* immunoprecipitated with PRG-1 in non-heat shocked animals serving as a positive control for RIP experiments in Fig 1e. Bars: mean value. Error bars: standard error. n = 4 biologically independent experiments. Statistical analysis: two-tailed unpaired t-test.

c. Representative micrographs of projected confocal Z-sections showing RNA FISH of *hsp-70 (F44E5.4/.5)* mRNA in WT and *prde-1* animals upon non heat shock (Ctrl) or heat shock. Note lack of expression in sperm. Compare with 22G-RNA expression in Fig 1h. Red: *hsp-70 (F44E5.4/.5)* mRNA. Blue: DAPI stained DNA. Scale bars: 100 μm (Ctrl, 30min HS) and 10 μm (Sperm).

d. Venn diagrams showing overlap between differentially expressed mRNAs and 22G-RNAs upon 5 minutes heat shock, and during 2 hours recovery from heat shock in WT and mutant backgrounds.

Suppl. Figure 3

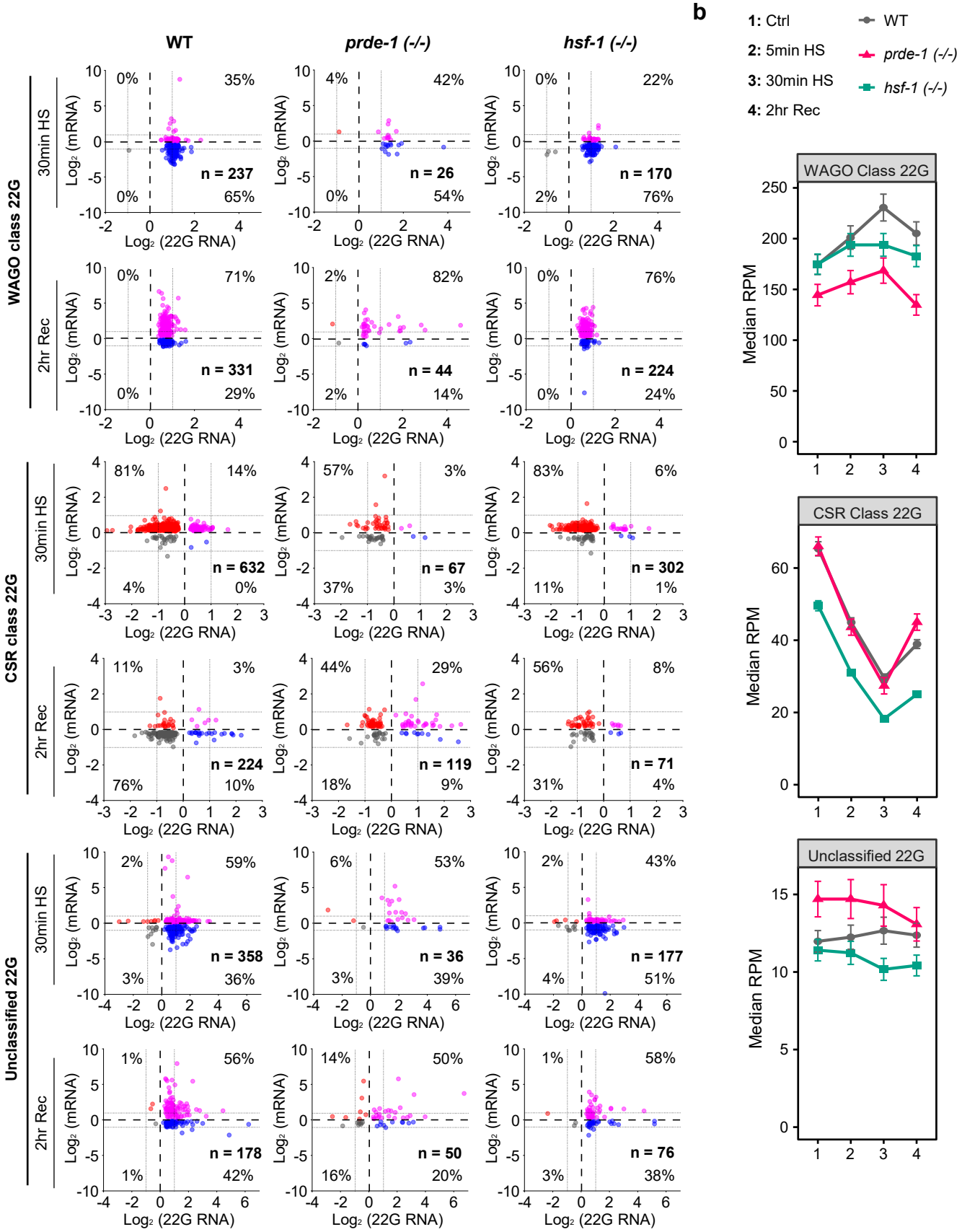

Supplementary Figure 3. piRNA-dependent WAGO and CSR-1 22G-RNAs and unclassified 22G-RNAs are templated from genes differentially expressed upon heat shock.

a. Scatter plot comparing the $\log_2$ fold-changes in WAGO class, CSR-1 class, and unclassified 22G-RNAs and complementary mRNAs in WT, *prde-1,* and *hsf-1*, upon 30min heat shock, and 2 hours recovery from heat shock. Number of mRNAs/category shown, and the % of mRNA in each quadrant of scatter plot shown.

b. Normalized expression (RPM) of WAGO and CSR-1 interacting 22G-RNAs, and unclassified 22G-RNAs in WT, *prde*-1, and *hsf-1* mutants. Y-axis: Expression (RPM). X-axis: Treatments (see top legend).

Suppl. Figure 4

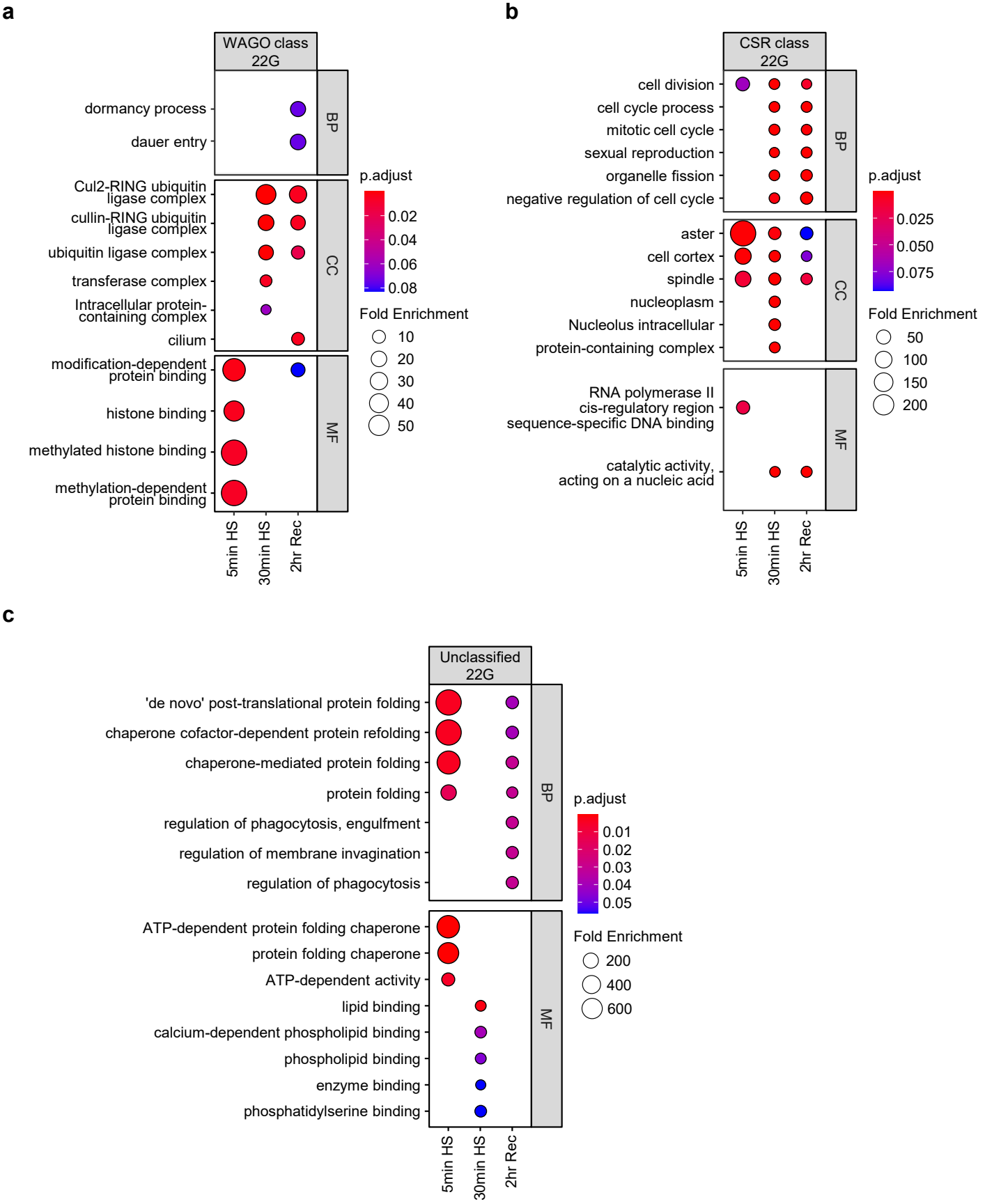

Supplementary Figure 4. 22G-RNAs produced upon heat shock target specific categories of mRNAs.

a-c. Gene enrichment analysis for **(a)** WAGO, **(b)** CSR-1, and **(c)** Unclassified 22G-RNA targets in WT animals across the different treatment conditions. All *hsp* genes are targets of unclassified 22G-RNAs (see Suppl. Table 4).

Suppl. Figure 5

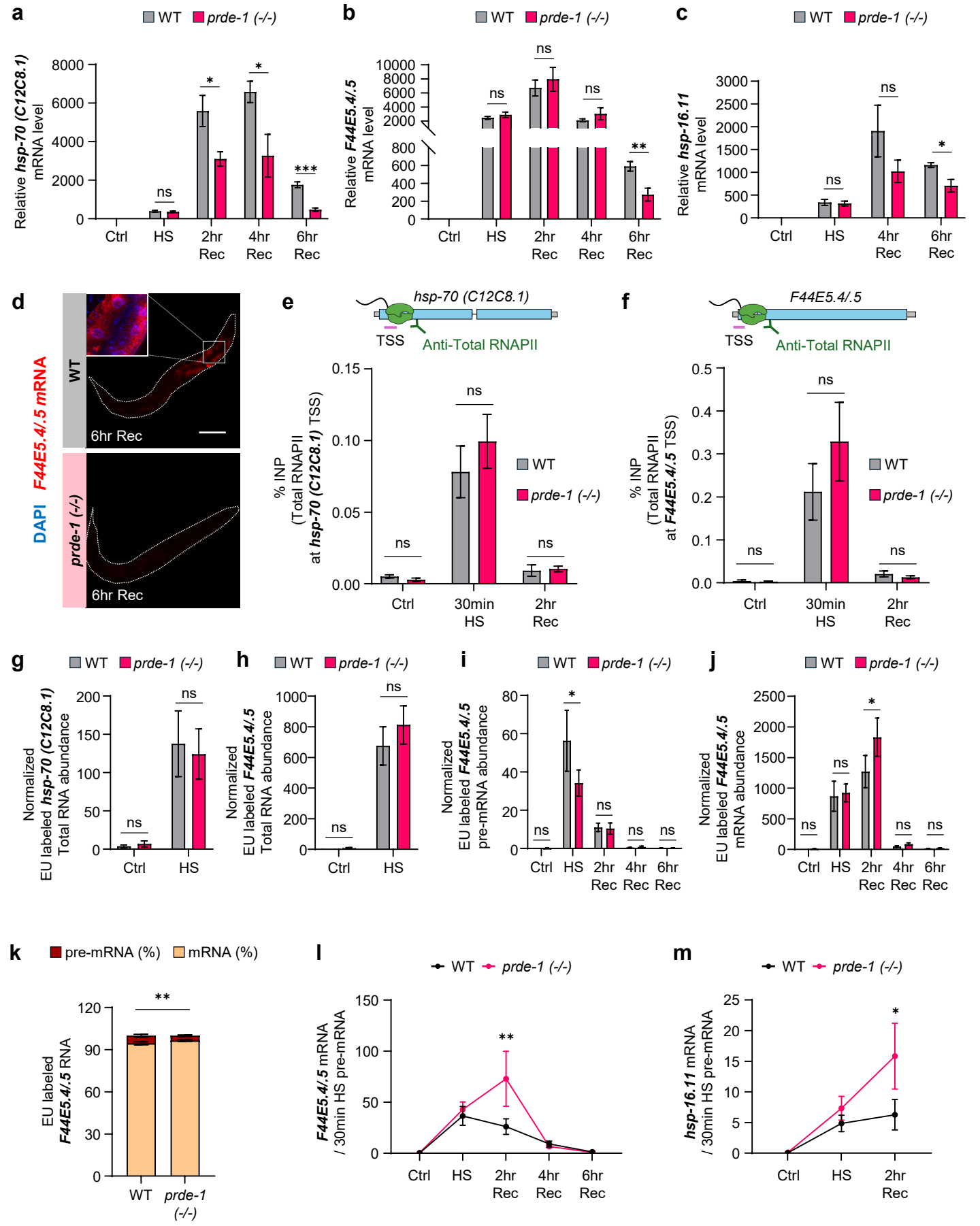

Supplementary Figure 5. The piRNA pathway protects *hsp* mRNAs persistence

a-c. RT-qPCR of relative fold change of *hsp-70s* (*C12C8.1* and *F44E5.4/.5*) and *hsp-16.11* mRNAs levels measured upon heat shock and recovery. mRNA values were normalized to *pmp-3* and shown relative to control (non-heat shocked) animals of each strain. Bars: mean value. Error bars: standard error. n = 3~13 biologically independent experiments. Statistical analysis: two-tailed unpaired t-test.

d. Representative micrographs of projected confocal Z-sections showing RNA FISH of *hsp-70 (F44E5.4/.5)* mRNA in WT and *prde-1* animals after 6 hours following heat shock. Red: *hsp-70 (F544E5.4/.5)* mRNA. Blue: DNA staining with DAPI. Scale bars: 100 μm

e, f. Total RNA polymerase II levels at *hsp* genes. **Top**: Schematic of *hsp-70 (C12C8.1* and *F44E5.4/.5)* gene, and region probed Transcription Start Site (TSS). **Bottom**: ChIP-qPCR showing fold enrichment over input. Y-axis: % ChIP input. X-axis: Treatments. Bars: mean value. Error bars: standard error. n = 3~4 biologically independent experiments. Statistical analysis: 2-way ANOVA.

g, h. Total nascent RNA abundance. EU-labeled **(g)** *hsp-70 (C12C8.1)* and **(h)** *hsp-70 (F44E5.4/.5)* RNA abundance. Y-axis: Normalized abundance. X-axis: Treatments. Bars: mean value. Error bars: standard error. n = 10~12 biologically independent experiments. Statistical analysis: 2-way ANOVA.

i, j. EU-labeled *hsp-70 (F44E5.4/.5)* **(i)** pre-mRNA and **(j)** mRNA abundance. Y-axis: Normalized abundance. X-axis: Treatments. Bars: mean value. Error bars: standard error. n = 5~13 biologically independent experiments. Statistical analysis: 2-way ANOVA.

k. Percentages of *hsp-70 (F44E5.4/.5)* pre-mRNA and mRNA in total EU-labeled RNA after 30min heat shock. Bars: mean value. Error bars: standard error. n = 13 biologically independent experiments. Statistical analysis: two-tailed unpaired t-test.

l. EU-labeled spliced *hsp-70 (F44E5.4/.5)* mRNAs produced from the nascent EU-labeled unspliced *hsp-70 (F44E5.4/.5)* pre-mRNA. Y-axis: Relative abundance. X-axis: Treatments. Line graph: mean value. Error bars: standard error. n = 5~14 biologically independent experiments. Statistical analysis: 2-way ANOVA.

m. EU-labeled spliced *hsp-16.11* mRNAs produced from the nascent EU-labeled unspliced *hsp-16.11* pre-mRNA. Y-axis: Relative abundance. X-axis: Treatments. Line graph: mean value. Error bars: standard error. n = 6~8 biologically independent experiments. Statistical analysis: 2-way ANOVA.

Suppl. Figure 6

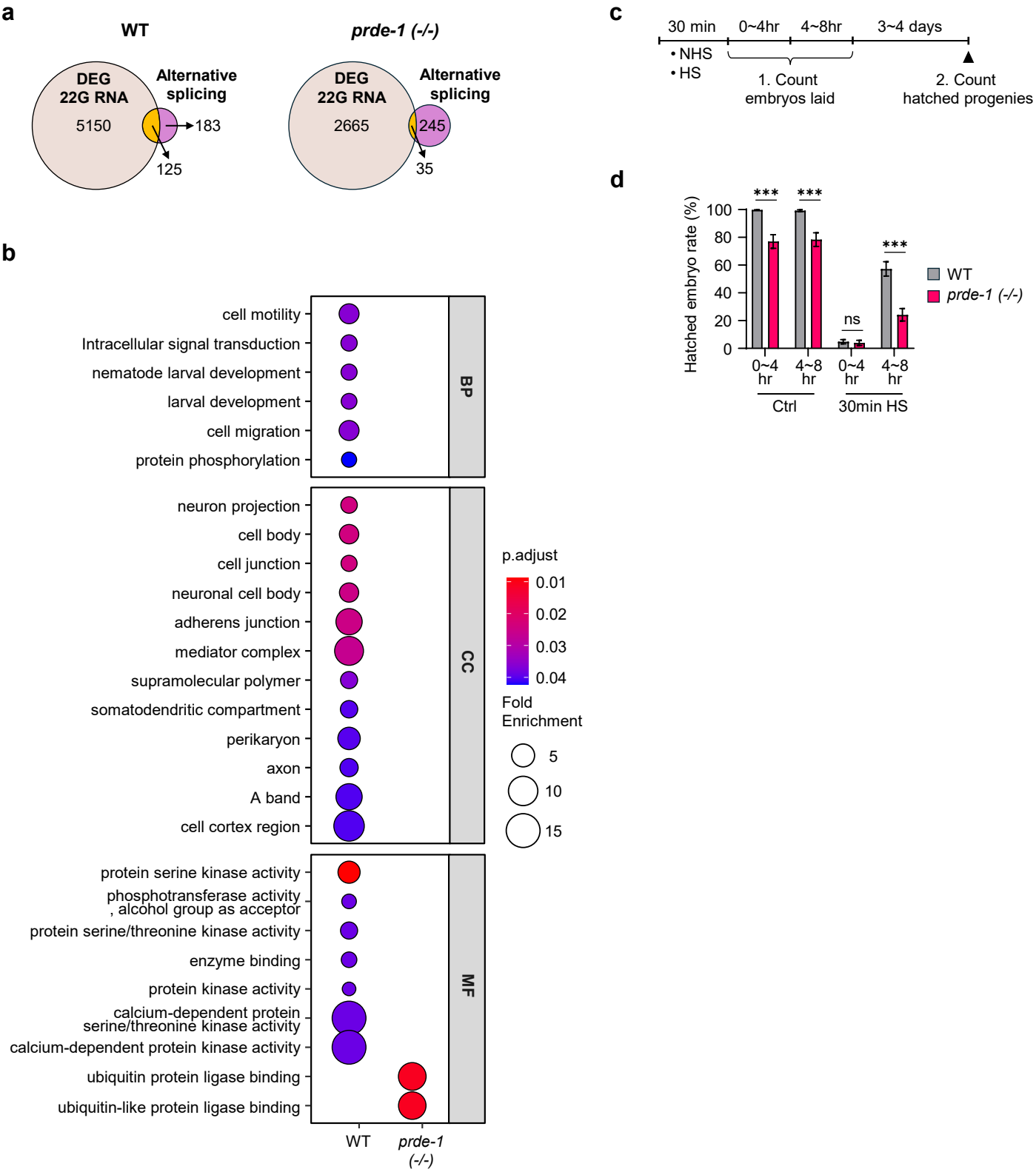

Supplementary Figure 6. Alternative splicing is affected in piRNA deficient (*prde-1*) animals.

a. Venn diagrams showing overlap between differentially expressed AS mRNAs and 22G-RNAs upon 30 minutes heat shock in WT and *prde-1* animals.

b. Gene enrichment analysis (p.adj <0.05) for AS mRNAs in WT and *prde-1* animals.

c, d. (c) Experiment schematic to assess recovery of fecundity in WT and *prde-1* animals after heat shock. NHS: non-heat shock. HS: heat shock. **(d)** Percentage of hatched embryos that laid over time during recovery from HS. Bars: mean value. Error bars: standard error. n = 7 biologically independent experiments. Statistical analysis: 2-way ANOVA.

Suppl. Figure 7

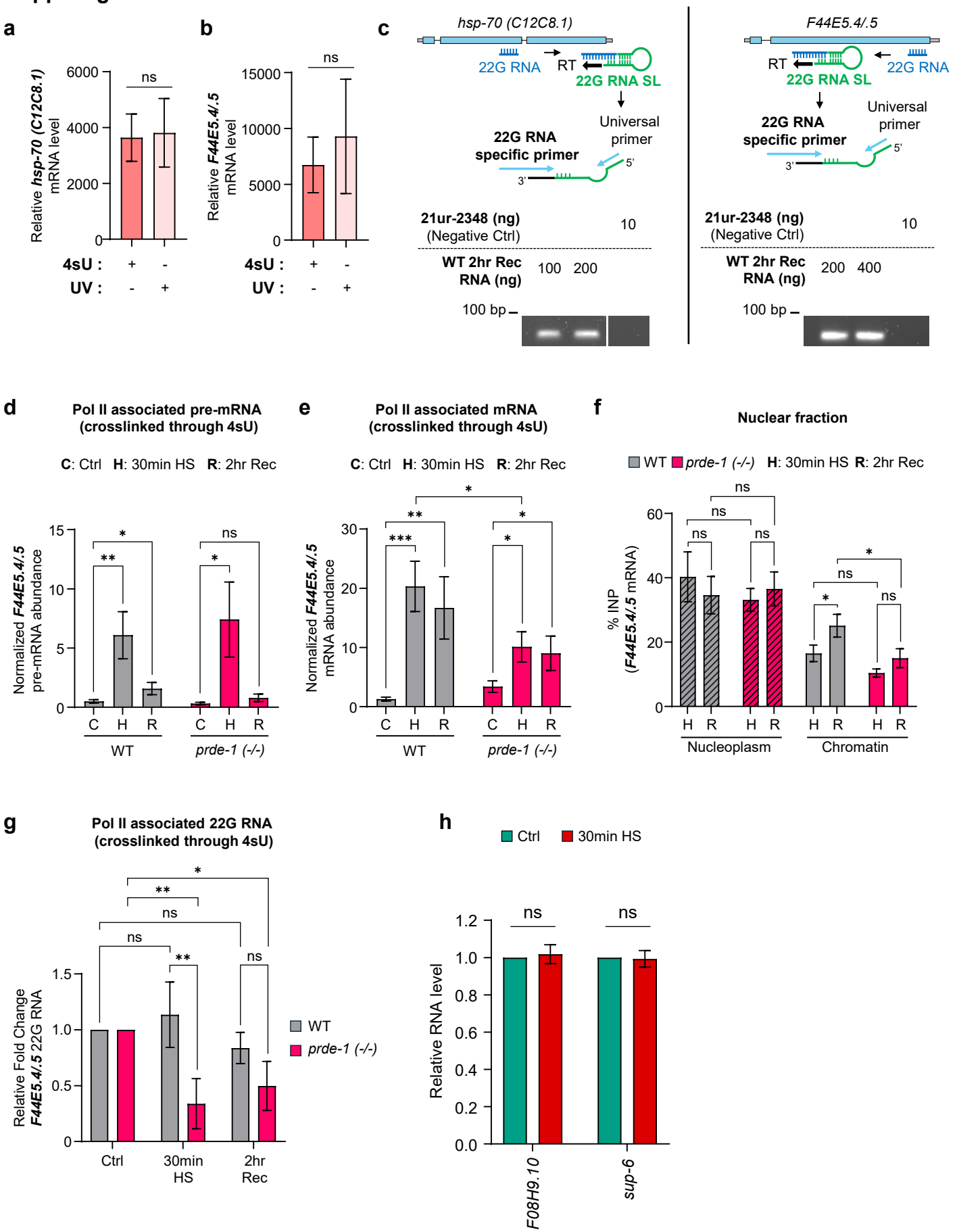

Supplementary Figure 7. 22G-RNAs associate with RNA Polymerase II and nascent *hsp* transcript to alter splicing.

a, b. 4sU treatment does not impair *hsp-70* expression. **(a)** *hsp-70 (C12C8.1)* mRNA and **(b)** *hsp-70 (F44E5.4/.5)* mRNA expressed upon heat shock in the presence and absence of either 4sU do not differ (UV exposure alone was used as comparison). Relative mRNA levels shown. mRNA values were normalized to *pmp-3* and shown relative to 4sU and UV-treated non-heat-shocked WT (value=1, not shown). Y-axis: Relative mRNA. X-axis: Treatment. Bars: mean value. Error bars: standard error. n = 3 biologically independent experiments. Statistical analysis: two-tailed unpaired t-test.

c. Stem loop RT-qPCR to amplify 22G-RNAs. **Top:** Cartoon depicting the 22G-RNA that was assayed, and complementary region on *hsp-70*. Universal primer, and 22G-RNA specific primers shown. **Bottom:** Representative agarose gel showing specificity. Different concentrations of total RNA containing 22G-RNAs were used to assess primer efficiency, and synthetically generated 21ur-2348 oligonucleotides were used as a negative control. See Materials and Methods for details. (expected PCR product size: 69bp)

d, e. Modified PAR-CLIP. Amounts of *hsp-70 (F44E5.4/.5)* **(d)** pre-mRNA and **(e)** mRNA that cross-linked to, and immunoprecipitated with Pol II normalized to *pmp-3* amounts. Y-axis: Normalized or relative abundance. X-axis: Treatment conditions (see top legend). Bars: mean value. Error bars: standard error. (d) n = 8~12 biologically independent experiments. Statistical analysis: two-tailed unpaired t-test; (e) n = 9~14 biologically independent experiments. Statistical analysis: two-tailed unpaired t-test (within strain) and 2 way-ANOVA (between strains).

f. Nuclear fractionation to assess amounts *hsp-70 (F44E5.4/.5)* RNA fate. Fold enrichment over input (nuclei) of *hsp-70 (F44E5.4/.5)* mRNA in respective fractions. Y-axis: % input (total nucleus). X-axis: Nuclear fraction, strain and treatment. Bars: mean value. Error bars: standard error. n = 9~10 biologically independent experiments. Statistical analysis: 2 way-ANOVA (within each fraction).

g. Amounts of *hsp-70* (*F44E5.4/.5*) 22G-RNA that cross-linked to, and immunoprecipitated with Pol II normalized to *pmp-3* amounts in the modified PAR-CLIP assay. Y-axis: Normalized abundance. X-axis: Treatments. Bars: mean value. Error bars: standard error. n = 4~6 biologically independent experiments. Statistical analysis: 2-way ANOVA.

h. Two other U1 RNA levels assessed upon heat shock. RT-qPCR of relative fold change in WT animals. Values normalized to *pmp-3* mRNA values and shown relative to non-heat-shock levels. X-axis: U1RNAs. Bars: mean value. Error bars: standard error. n = 3 biologically independent experiments. Statistical analysis: 2-way ANOVA.

Suppl. Figure 8

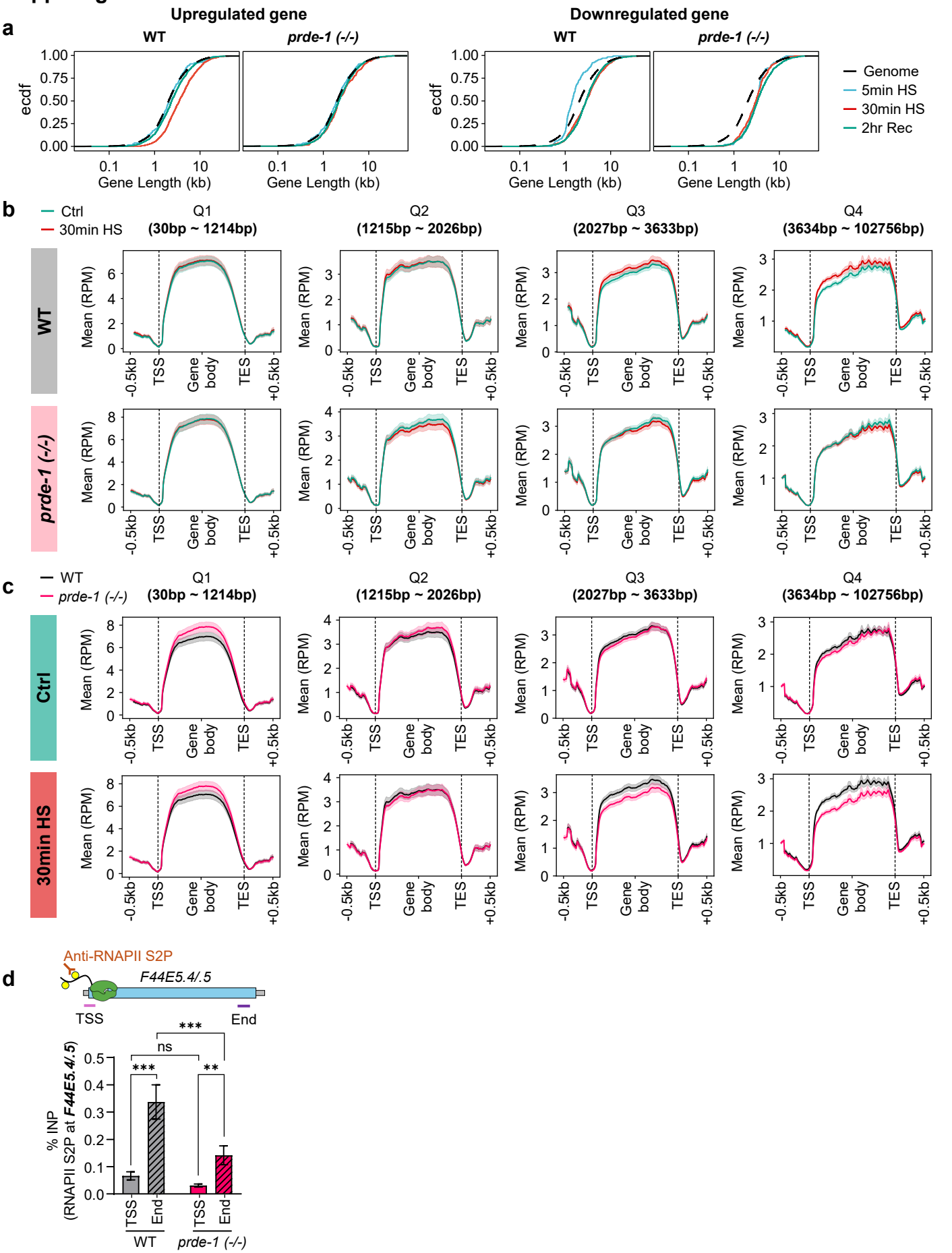

Supplementary Figure 8. piRNA pathway affects gene expression in a a gene-length dependent manner.

a. Empirical Cumulative Distribution Function (ECDF) plots, to visualize the proportion of gene expression values (mRNA-seq) as a function of gene lengths. Expression values of genes significantly upregulated and downregulated upon 30min heat shock (p.adj <0.05) in wild-type (WT) and *prde-1* are plotted. Y-axis: Cumulative proportion of reads. X-axis: Gene lengths. **Top:** Strain names and differential expression. Note bias towards increased gene lengths in WT, but not *prde-1* upregulated genes, but similar bias towards long genes in all downregulated genes.

b, c. Metagene plot showing mRNA expression (mRNA-seq) stratified by gene length compared between control and upon 30 min. heat shock, **(b)** within strains, and **(c)** between strains.

d. Elongating RNA polymerase II (anti-S2P) levels at *hsp* genes. **Top**: Schematic of *hsp-70* (*F44E5.4/.5*) gene, and regions probed: Transcription Start Site (TSS) and distal regions (3') of *hsp-70* (*F44E5.4/.5*). **Bottom:** ChIP-qPCR showing fold enrichment over input. Y-axis: % ChiP input. X-axis: Strain, and region assayed. Bars: mean value. Error bars: standard error. n = 8 (TSS) and 4 (End) biologically independent experiments. Statistical analysis: 2 way-ANOVA.

Suppl. Figure 9

a

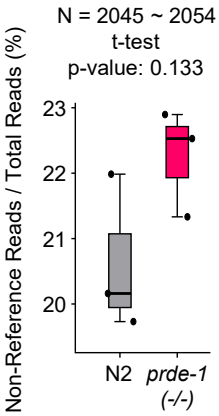

Supplementary Figure 9. piRNAs protect transcript fidelity.

a. Percentage of variant containing mRNA molecules in wild type and *prde-1* mutants. Y-axis: % variants. X-axis: Strain. Total variant containing sites=2045-2054. Approximately 2.7 x 10^7 individual mRNAs analyzed. See **Methods** for details. Boxplots: median value depicted. Error bars: standard error. Statistical analysis: two-tailed unpaired t-test.

C. ELEGANS STRAINS AND GROWTH CONDITIONS

C. elegans used in all experiments are listed in Table 1. Strains were obtained from the *Caenorhabditis Genetics Center* (CGC, Twin Cities, MN), generated in the Prahlad laboratory, or generated by SunyBiotech (Suzhou, Jiangsu, China). All crossed worms were verified by genotyping. The primers used in genotyping are listed in Table 2.

All strains were maintained at 20°C on nematode growth media (NGM) plates. NGM plates were prepared by pouring 8.9 ml autoclaved liquid NGM per 60 mm plate. NGM was allowed to solidify at room temperature (RT) for 2 days, seeded with 300 µl OP50 *E. coli* (O.D = 1.8~2.0), and dried at RT for no more than 2 days. Population densities were matched based on growth rate of the strains. To maintain healthy continuously growth populations, 10~15 animals at larvae stage 4 (L4) were passed onto a new plate every 4 days. For experiments, day-one adult animals were used. These were generated either by picking L4-stage worms and harvesting them 24~24 hrs later, or by bleach-hatching and collecting day-one adults worms 82~84 hrs later, depending on experimental requirements.

HEAT SHOCK

Worms were exposed to acute heat stress as previously described in Das et al., elife 2020[1]. Briefly, NGM plates containing day-one adults were sealed with parafilm and immersed in a water bath pre-warmed to 34°C for different duration as mentioned. For recovery experiments, NGM plates were incubated at 20°C incubator immediately after heat shock and harvested after specific times mentioned in the experiments.

RNA SEQUENCING

RNA Library Preparation

26 For RNA-sequencing, three independent biological replicates of each strain and each treatment
27 were harvested and processed as described. For each sample/treatment, approximately 200
28 L4-stage worms were transferred to OP50 plates. After 26~27hrs, worms from two plates per
29 condition [non-heat shock (NHS), 5min HS, 30min HS, and 30min HS + 2hr Rec] were collected
30 in nuclease-free water. Total RNA was extracted using the Mirvana miRNA Isolation Kit
31 (Invitrogen; Cat #AM1560). Genomic DNA in the sample was removed using Turbo DNA-free Kit
32 (Invitrogen; Cat #AM1907). RNA was separated by size into mRNA (>200 nt) and small RNA
33 (<200 nt). Small RNA samples were treated with 10U RppH (NEB; Cat #M0356S) at 37°C for 30
34 min, then purified using the Zymo RNA Clean & Concentrator kit (Zymo Research; Cat #R1015).
35 RNA concentrations were measured with a Qubit 4 fluorometer (Thermo Scientific). mRNA
36 libraries were prepared using the KAPA mRNA Hyperprep kit (Roche; Cat #08098123702);
37 small RNA libraries were prepared using the Illumina TruSeq Small RNA Library Preparation kit
38 (Illumina; Cat #RS-200), following manufacturer's protocol.
39
40 ***Small RNA analysis***
41 Small RNA data was analyzed using the tinyRNA[2] (v1.50) pipeline with its default configuration.
42 The process included adapter trimming and quality filtering with fastp[3], followed by genome
43 alignment to the *C. elegans* genome (release WS279) using Bowtie[4]. An additional setting,
44 counter_decollapse: True, was specified to generate decollapsed SAM files.
45 The module tiny-count was used to count the different types of small RNA according to the
46 selection rules specified in the following table.

Select for...	with value...	Classify as...	Hierarchy	Overlap	Strand	5'End Nucleotide	Length
Class	risiRNA	rRNA	1	Partial	both	all	all

Select for...	with value...	Classify as...	Hierarchy	Overlap	Strand	5'End Nucleotide	Length
Class	miRNA	miRNA	2	5'Anchored, 0, 4	sense	all	all
Class	piRNA	piRNA	2	5'Anchored	sense	all	18-21
Class	CSR	CSR Class 22G	3	Partial	antisense	G	21-23
Class	WAGO	WAGO Class 22G	3	Partial	antisense	G	21-23
Class	ALG	ALG Class 26G	3	Partial	antisense	G	26
Class	ERGO	ERGO Class 26G	3	Partial	antisense	G	26
Class	ALG	ALG target 22G	3	Partial	antisense	G	21-23
Class	ERGO	ERGO target 22G	3	Partial	antisense	G	21-23
Class	unk	unclassifed 22G	3	Partial	antisense	G	21-23
Class	unk	unclassifed siRNA	4	Partial	both	all	21-24

The read counts obtained from tiny-count were used to generate genome-wide coverage profiles for the 22G-RNAs and piRNA. The coverage was normalized as Read per million (RPM) and output as BigWig (bw) files using rtracklayer[5]. Differential Expression was computed by using a modified version of tyny.deseq.r, the R module was adjusted to remove the ribosomal RNA (rRNA) from the analysis, and to calculate the gene expression in RPM in addition to

53 DESeq normalized counts. Changes in expression were presented as log_2 fold-change, and
54 genes with an adjusted p-value of <0.05 (after correction with Benjamini & Hochberg)[6], were
55 considered significant.
56
57 ***mRNA seq analysis***
58 RNA-seq samples were analyzed and processed using the nf-core/rnaseq (v3.12.0) pipeline,
59 which was executed with Nextflow[7] (v22.10.6). Sequence quality was assessed with FastQC
60 [8](v0.11.9), and low-quality reads and adapters were removed using Trimmomatic[9] (v0.67). The
61 processed reads were then aligned to the *C. elegans* genome (WBcel235, Ensembl release
62 111) with STAR[10] (v2.7.9a) using default settings. Alignments were quantified against the
63 WBcel235 annotation with Salmon (v1.9.0). Alignment quality control was performed with
64 Qualimap[11] (v2.2.2) and RSeQC[12] (v3.0.1).
65
66 ***Differential Expression***
67 Differential expression analysis was performed between RNA-seq samples using **DESeq2** with
68 the **Wald test**. Expression changes were presented as log2 fold-change. Genes with an adjusted
69 p-value <0.05, following correction with the **Benjamini & Hochberg**[6] method, were considered
70 significantly differentially expressed.
71
72 ***Analysis of Alternative Splicing Events***
73 To identify differential alternative splicing events, RNA-seq data were re-processed using the nf-
74 core/rnasplice (v1.0.4) workflow. This pipeline was executed with Nextflow (v23.10.0) and relied
75 on reproducible software environments from Bioconda and Biocontainers.
76
77 Within the rnasplice pipeline two modules were used to detect differential splicing and calculate
78 the Percent Spliced-In (PSI) for each event, SUPPA2[13] (v2.3) and rMATS (v4.1.2)., Splicing

events were considered significant if the absolute difference in PSI (dPSI) between the 30 minutes heat shock and control conditions had a p-value <0.1.

Formula : $\boldsymbol{\Psi} = \sum(\boldsymbol{TPMinclusion}) + \sum(\boldsymbol{TPMexclusion}) \sum(\boldsymbol{TPMinclusion})$ [13]

Pearson's Chi-squared test with Yates' correction was used to determine if the number of up- or down-regulated splicing events during heat shock differed between the N2 and PRDE1 strains (p-value <0.05).

Differential Transcript Usage (DTU) analysis was performed using SUPPA2. First, usage of transcripts (isoforms) were tested for significant differences between conditions. Isoforms with a p <0.1 were considered significant. For analysis and visualization, the average Percent Spliced In (PSI or Ψ) value for each isoform was calculated across the biological replicates within each condition. The resulting list of PSI per isoforms was then filtered to retain only those occurring in genes previously identified as differentially expressed (DEGs). Student t-test was used to compare the means between the conditions at significance level p <0.05.

Formula: $\boldsymbol{PSI_i} = (\boldsymbol{TPM_i})/(\boldsymbol{\Sigma_(j = 1)\hat{}n\ TPM_j})$ [13]

Gene Ontology

Gene Ontology analysis was performed by using Over Representation Analysis (ORA), with the R package ClusterProfiler[14,15]. GO annotations for *C. elegans* were obtained from R package org.Ce.eg.db: Genome wide annotation for Worm[16] (version 3.18.0). Ontology terms enriched with an adjusted p-value <0.05 or <0.1 (Benjamini & Hochberg)[6] were considered significant. Fold-Enrichment was calculated as the ratio of the frequency of input genes annotated in a GO term to the frequency of all genes annotated to that term[14].

Data Visualization

105 The metaprofiles were generated using Deeptools[17] (v3.56) by normalizing the coverage by
106 RPM per bp) and then modified to plot them using R.
107
108 Venn diagrams were generated using the Eulerr[18] package (v.7.0.2) in R[18]. Additional plots were
109 generated using ggplot2 (v.3.5.1)[19] .
110
111 **RNA FISH**
112 ***mRNA FISH***
113 RNA FISH was performed as previously described[20]. Probes were designed against mRNA
114 according to the Biosearch Technologies website, and consisted of 25-35 11bp sequences that
115 complementary to the *hsp-70s (C12C8.1* and *F44E5.4/.5)* mRNA. For mRNA FISH, about 20
116 day-one adult worms were harvested in 1x PBS and fixed in 4% paraformaldehyde (Electron
117 Microscopy Science; Cat #50-980-487) for 45 mins. After two washes with 1x PBS, worms were
118 permeabilized in 70% ethanol at 4°C for 24~26 hrs. Worms were washed with Stellaris Buffer A
119 (Biosearch Technologies, Cat # SMF-WA1-60) and incubated at 37°C for 16 hrs in hybridization
120 buffer (Cat #SMF-HB1-10) containing 0.2 mM FISH probes targeting *hsp-70s (C12C8.1* and
121 *F44E5.4/.5)* mRNA. After washing three times with pre-warmed Wash Buffer A and one time
122 with Wash Buffer B (Biosearch Technologies, Cat # SMF-WB1-20), worms were mounted in
123 Vectashield with DAPI (Vector Laboratories; Cat #H-1200-10). Imaging was performed using a
124 Leica TCS SPE Confocal Microscope with 20x dry and 63x oil objectives, and LAS AF software.
125
126 ***22G RNA FISH***
127 For 22G-RNA FISH, animals were processed as described above for mRNA FISH.
128 Fluorescence conjugated probes targeting 22G-RNAs were purchased from IDT, and were
129 complementary to one of the most abundant 22G-RNAs identified by sRNA-seq (hence they

130 were in the sense direction as mRNA, and could not hybridize to mRNA). 0.2 μM FISH probe
131 targeting *F44E5.4/.5* 22G RNA was used per slide. Sequence of the probe is in Table 3.
132
133 **AUXIN-INDUCIBLE DEGRADATION (AID) TREATMENT**
134 Auxin plates were prepared at a final concentration of 4 mM by adding indole-3-acetic acid (Alfa
135 Aesar; Cat #A10556), dissolved in ethanol at 400 mM, to autoclaved NGM that had cooled to
136 approximately 55°C prior to pouring. NGM plates with ethanol served as controls. Plates were
137 dried at RT for 2 days, then for 2 more days after seeding with 300 μl OP50 (O.D = 1.8~2.0).
138 About 20 day-one adults were transferred to OP50-seeded auxin or ethanol plates and
139 incubated at 20°C for 4 hrs. Worms were then either not heat shocked (NHS) or subjected to
140 heat shock (HS) for 30mins at 34ºC and processed for FISH as above.
141
142 **IMMUNOSTAINING**
143 Immunostaining of dissected gonad was performed as previously described[20] . 10~15 day-one
144 adults were picked into 15 μl 1x PBS on a cover glass (Leica Biosystem; Cat #3800105) and
145 dissected with a surgical blade #11. Dissected worms were fixed in 4% paraformaldehyde for 6
146 mins. A charged slide (Epredia; Cat #4951PLUS-001) was placed over the cover glass, then
147 quickly transferred onto a metal block that had been cooled with dry ice for over 10mins. After
148 quickly removing the cover glass, samples were post-fixed in 100% methanol pre-chilled at
149 −20°C for 2mins, washed in 1x PBST (1x PBS with 0.1% Tween-20), and then blocked in 1x
150 PBST with 0.5% BSA for 1 hr. Samples were incubated at 4°C overnight with Mouse anti-FLAG
151 M2 (Sigma-Aldrich, Cat #F3165-1MG), diluted 1:2,000 in 1x PBST. Following washing, samples
152 were incubated at RT for 2 hrs with Donkey anti-Mouse Alexa Fluor 488 (Invitrogen; Cat
153 #A32766), diluted 1:500 in 1x PBST. After washing, samples were mounted in the Vectashield
154 with DAPI and imaged.
155

156 **RNA ISOLATION AND QUATIFICATION OF RNA LEVELS BY RT-qPCR**

157 RNA was extracted from 30~40 day-one adults exposed to indicated heat shock durations and
158 recovery times. Animals were collected in 50 µl Trizol and immediately snap-frozen in liquid
159 nitrogen. Samples were thawed on ice, mixed with 200 µl Trizol, and lysed using Precellys 24
160 homogenizer. RNA was isolated from lysates with chloroform and precipitated with isopropanol
161 and glycogen. After washing with 70% EtOH, RNA pellet was dissolved in nuclease-free water
162 and treated with TURBO DNase. cDNA was synthesized using iScript cDNA synthesis kit (Bio-
163 Rad; Cat #1708891). qPCR was performed using PowerUp SYBR Green Master Mix (Applied
164 Biosystems; Cat #A25742) on a QuantStudio 3 Real-time PCR System (10 µl reaction, 96-well
165 plate).

166

167 The amounts of RNA were quantified using one of the following methods:

168 ***mRNA RT-pPCR***

169 (i) Relative quantification using the ΔΔCt method: mRNA (exon-exon junction primers), and pre-
170 mRNA (intron-exon primers) levels were computed relative to *pmp-3* (previously verified by use
171 to remain steady during heat shock)[1], which served as an internal control. Primer locations are
172 depicted in the Method Fig 1 below and primer sequences are in Table 2.

173 (ii) Absolute quantification using standard curves: Absolute amounts of pre-mRNA and mRNA
174 were estimated through the generation of standard curves using serial dilutions of defined
175 concentrations of *hsp-70 (C12C8.1)* and *F44E5.4/.5* mRNA, pre-mRNA, as well as *pmp-3*
176 mRNA. The mRNA and pre-mRNA used to generate each standard curve, was obtained by
177 PCR amplification from cDNA or genomic DNA extracted from whole worms, PCR amplified
178 using primers external to the primer target sites used in the experiments, gel purification, and
179 quantification using a Qubit 4 fluorometer. qPCR was conducted using 10-fold serial dilutions of
180 a known concentration of purified PCR products. The standard curves were created from the CT
181 values obtained from the dilutions (see Method Fig 1).

182 The amounts of mRNA and pre-mRNA were extrapolated derived from these curves using the

183 formula.

184 **Formula:** $\boldsymbol{Absolute\ amount\ of\ RNA = Inital\ Con. \times 10^{\left(\frac{CT\ Value - constant}{slope}\right)}}$

185 To account for differences in lysis efficiency, variations in harvesting of animals, and other

186 factors, a similar curve was calculated for *pmp-3* and the final values were normalized to *pmp*-3

187 values known to remain stable through heat shock[1].

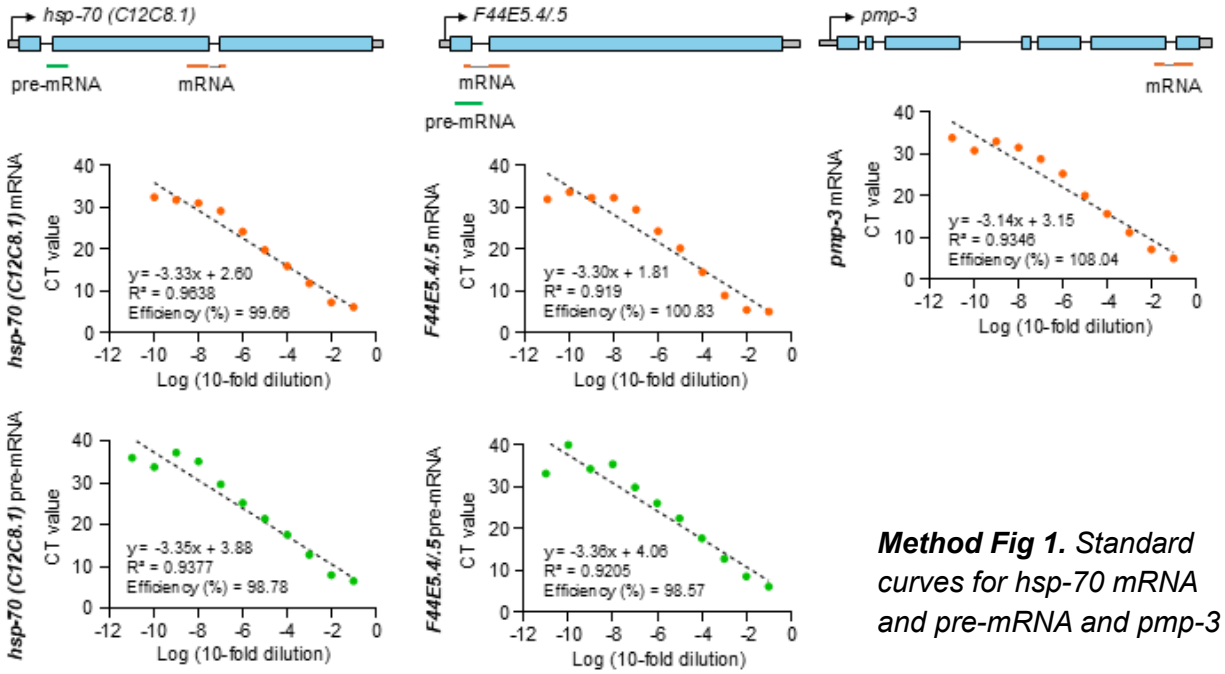

Method Fig 1. *Standard curves for hsp-70 mRNA and pre-mRNA and pmp-3*

188

189 The primers used for qPCR analysis are designed using Primer 3 software and generated by

190 Integrated DNA Technologies (See **Table 2**).

191

192 ***SMALL RNA (sRNA) RT-qPCR***

193 Small RNA qPCR was performed using stem-loop RT-qPCR by modifying published protocols[21]

194 Total RNA extracted from animals, or immunoprecipitated after 4sU treatment and RNAPII

195 immunoprecipitation (see below), incubated with 50 nM 22G RNA-specific stem loop primer at

196 70°C for 5mins, cooled on ice for ≥5 mins. cDNA was synthesized using 100U Superscript II
197 Reverse Transcriptase (Invitrogen; Cat #18064014) in 1x reaction buffer, 1U SUPERase-In
198 RNase inhibitor, and 0.5 mM dNTPs. The RT-qPCR mix included 2 µl cDNA, 0.25 µM 22G RNA-
199 specific forward primer, 0.25 µM universal reverse primer,1x PowerUp SYBR Green Master Mix.
200 Relative fold change of 22G-RNA was quantified relative to immunoprecipitated *pmp-3* using the
201 ΔΔCt method. Primer specificity was tested using a synthetic sRNA (21ur-2348). Specificity of
202 the reaction was verified by running out the reaction on agarose gels. Representative gel and
203 PCR design are shown in Suppl. Fig 7c. The sequence of primers is listed in Table 3.
204
205
206 **ChIP-qPCR**
207 Chromatin immunoprecipitation (ChIP) was performed as previously described[20] . Following
208 exposure to one of three conditions (NHS, 30min HS, or 30min HS + 2hr Rec), approximately
209 700 day-one adults, synchronized by bleach hatching, were harvested in 1x PBS and
210 crosslinked with 2% formaldehyde at RT for 10 mins. Crosslinking was quenched with 250 mM
211 Tris (pH 7.4) for 10 mins. Samples were washed three times in ice-cold 1× PBS containing
212 protease inhibitor cocktail (PIC; Thermo Scientific; Cat #78429) and then snap-frozen in liquid
213 nitrogen. Pellets were resuspended in 200 µl FA buffer (50 mM HEPES/KOH (pH 7.4), 150 mM
214 NaCl, 50 mM EDTA, 1% Triton X-100, 0.1% sodium deoxycholate, 0.5% sarkosyl) freshly
215 supplemented with 1 mM DTT and 1x PIC. Worms were lysed using a Precellys 24
216 homogenizer and sonicated (Bioruptor Pico; 8~10 cycles of 30sec on/off). Debris was removed
217 by centrifugation (13,500 rpm at 4°C for 5 mins). Protein A/G Magnetic Beads (20 µl per sample;
218 Thermo Scientific, Cat #88803) were washed two times with FA buffer. To eliminate non-specific
219 binding, 5 µl of beads were then added to the lysates and incubated at 4°C for 1 hr. 10% of the
220 pre-cleared lysate was kept as input, and the rest was incubated overnight at 4°C with anti-total
221 RNAPII (Diagenode; Cat #C1520004) or RNAPII s2P (Diagenode; Cat #15200005), followed by

222 3 hrs incubation with 15 µl beads. Beads were washed sequentially with low salt, high salt, LiCl,
223 and TE buffers, then eluted in 150 µl elution buffer (10 mM EDTA, 1% SDS, 0.1 M sodium
224 bicarbonate). Elutes and volume-matched inputs were de-crosslinked overnight with 0.8U
225 proteinase K (NEB; Cat #P8107S) and 160 mM NaCl. DNA was purified using
226 phenol/chloroform/isoamyl alcohol. qPCR was performed as above. All experiments were
227 expressed as % input value. The sequence of the primers used for ChIP experiments are listed
228 in Table 2 and depicted in Fig 3j; Suppl. Fig 5e, f, and 8d.
229
230 **RNA IMMUNOPRECIPITATION (RIP) FOLLOWED BY RT-qPCR**
231 RNA immunoprecipitation (RIP) was performed with ~700 day-one adults per condition,
232 expressing FLAG::FRG-1 (endogenous PRG-1 tagged with FLAG epitope using CRISPR/Cas9)
233 synchronized by bleach hatching. To account for the non-specific interactions of the abundant
234 *hsp* mRNA generated by heat shock, we used wild-type (N2) animals not expressing FLAG as a
235 negative control, and compared specific immunoprecipitation (IP) of PRG-1 IP to this non-
236 specific IP. RIP was conducted in the absence of cross-linking. Worms were harvested in
237 nuclease-free water, pelleted, and snap-frozen in liquid nitrogen. Worms were resuspended in
238 FA buffer with 1 mM DTT, 1x PIC, and 0.01U/µl SUPERase-In RNase inhibitor (Invitrogen; Cat
239 #AM2696), then lysed and sonicated (2 cycles of 30 sec on/off). 10% of the pre-cleared lysate
240 was kept as input, and the rest was incubated with anti-FLAG M2 (Sigma-Aldrich, Cat #F3165-
241 1MG) at 4°C for 2~3 hrs, followed by beads for 1hr. After washing, beads were eluted with
242 elution buffer containing 0.01U/µl SUPERase-In RNase inhibitor. Elutes and volume-matched
243 inputs were de-crosslinked by incubating them with 0.8U proteinase K (NEB; Cat #P8107S) at
244 45°C for 1hr. RNA was isolated using Trizol and qRT-PCR was performed as above. Because
245 we were had no reason to expect that *pmp-3* would also bind to PRG-1, and be
246 immunoprecipitated, to control for variation in harvesting, lysis, loading etc., we normalized *hsps*
247 in IP sample to *pmp-3* in the input sample using the ΔΔCt method. *bath-45*, known to interact

248 with PRG-1 was used as a positive control for the efficacy of RIP. The sequence of the primers
249 used for RIP experiments are listed in Table 2.
250
251 **4sU RNAPII IP qPCR**
252 All procedures for 4sU RNAPII immunoprecipitation (IP) are outlined in Fig 3a. Specifically, 4sU
253 was delivered as a liquid suspension mixed with bacterial food. The bacterial food, OP50, was
254 heat-killed to minimize its metabolism of 4-Thiouridine (4sU). To most optimally deliver 4sU
255 within a short time, about 700 day-one adult worms were rapidly collected in nuclease-free
256 water and then resuspended in S-basal containing 10mg/ml heat-killed OP50 and 4mM 4sU
257 (Sigma Aldrich; Cat #T4509). The suspension was seeded onto empty NGM plates to prevent
258 hypoxia (a critical step since *C.elegans* suspended in liquid media have a markedly different
259 heat shock response). The worms, bacteria and 4sU were allowed to dry at RT for 1hr, and
260 subjected to one of three conditions [not heat shocked (NHS), heat shocked at 34ºC for 30 mins
261 (30min HS), or heat shocked at 34ºC for 30 mins and allowed to recover for 2 hrs at 20ºC
262 (30min HS + 2hr Rec)], and then crosslinked by exposure to UV (365 nm) for 30 sec. Samples
263 were harvested in nuclease free water and snap-frozen in liquid nitrogen. Worm lysis,
264 immunoprecipitation, RNA isolation, and qRT-PCR followed the RIP-qRT-PCR protocol, using
265 anti-total RNAPII (Diagenode; Cat #C1520004) instead of anti-FLAG. To quantify mRNA and
266 pre-mRNA, absolute amounts of RNA were estimated from standard curves and normalized by
267 immunoprecipitated *pmp-3*.
268
269 **EU LABELLING OF NASCENT RNA**
270 To examine the expression patterns of nascent *hsp* genes we used a pulse-chase approach
271 using the Click-iT Nascent RNA Capture Kit (Invitrogen; Cat #C10365) according to the
272 manufacturer's instructions, to label RNA. In brief, 50 day-one adult worms were placed on an
273 OP50 bacterial lawn containing 4 mM EU and incubated at 20°C for 10 mins to preload them

274 with EU. Subsequently, the worms were incubated at 20°C (serving as controls) or underwent
275 heat shock for 30 mins at 34ºC. Control and heat shocked animals were harvested in 50 µl
276 Trizol and immediately snap-frozen in liquid nitrogen. To assess maturation of pre-mRNA to
277 mRNA, animals were allowed to recover in the absence of EU. For this, worms were
278 transferred, immediately after heat shock, from EU containing OP50 plates onto new NGM
279 plates seeded with regular OP50. The plates were then incubated at 20°C for 2, 4, or 6 hours,
280 and subsequently harvested in Trizol. RNA isolation was performed as described in the RT-
281 qPCR protocol. EU-labeled RNA was biotinylated with 0.4 mM biotin azide and purified by
282 reprecipitating. The biotinylated RNA was captured using 12 µl of streptavidin beads. cDNA
283 synthesis was carried out directly on the beads containing nascent RNA using the iScript cDNA
284 synthesis kit. qPCR was processed as described in the RT-qPCR protocol. To quantify mRNA
285 and pre-mRNA, absolute amounts of RNA were estimated from standard curves. To assess
286 maturation from pre-mRNA to mRNA, mRNA expression level at each time point was divided by
287 pre-mRNA expression at 30min HS. In both analysis, mRNA and pre-mRNA expression
288 amounts were quantified relative to EU labeled *pmp-3* amounts.
289
290 **SUBCELLULAR FRACTIONATION**
291 Subcellular fractionation was performed with ~700 day-one adults per condition synchronized
292 through bleach hatching method. Worms were harvested in 1.5 ml tube with nuclease free
293 water, pelleted and snap-frozen in liquid nitrogen. Frozen pellet was washed with 500 µl
294 hypotonic buffer (15 mM HEPES/KOH (pH7.5), 10 mM KCl, 5 mM MgCl2, 0.1 mM EDTA, 350
295 mM Sucrose). Worms were resuspended in 100 µl hypotonic buffer supplemented with 1 mM
296 DTT, 1x PIC and 0.01U/µl SUPERase-In RNase inhibitor and homogenized by pestle (SP Bel-
297 Art ; Cat #F19923-0001). To remove worms' bodies and debris, homogenates were centrifuged
298 at 500 xg at 4°C for 5 mins, and supernatant was transferred to a new 1.5 ml tube. The
299 supernatant was then centrifuged at 4,000 xg at 4°C for 5 mins to collect nucleic (pellet) fraction.

300 The nuclei pellet was washed three times with 200 µl hypotonic buffer. After last washing, the
301 pellet was resuspended in 120 µl nucleus lysis buffer (50 mM Tris (pH7.5), 140 mM NaCl, 1.5
302 mM MgCl2, 0.5% (w/v) NP-40) supplemented with 1 mM DTT, 1x PIC and 0.01U/µl SUPERase-
303 In RNase inhibitor, and incubated in ice for 20 mins. 20 µl of sample was aliquoted to a 1.5 ml
304 tube labelled as "input", and the remaining samples were centrifuged at 20,000 xg at 4°C for 10
305 mins. The supernatant was transferred to a 1.5 ml tube labelled as "nucleoplasm". The pellet
306 was resuspended in 100 µl high salt solution (10 mM Tris (pH7.5), 700 mM NaCl) supplemented
307 with 1 mM DTT, 1x PIC and 0.01U/µl SUPERase-In RNase inhibitor, and incubated in ice for 20
308 mins, and centrifuged at 20,000 xg at 4°C for 5 mins. The supernatant was transferred to a 1.5
309 ml tube labelled as "Chromatin". The RNA in each sample was isolated using Trizol, and *hsp*
310 gene expression level was measured as described in the RT-qPCR protocol. The results of
311 experiments were presented as percentage input values.
312
313 This method of extraction did result in the loss of some nuclei. Nevertheless, the nuclei
314 obtained were 'clean' and not contaminated with cytoplasmic fractions, confirmed by conducting
315 a Western blot and probing for tubulin.
316
317 **RNA INTERFERENCE (RNAi)**
318 RNAi experiments were conducted using the standard feeding RNAi methods. Bacterial clones
319 expressing the control (empty vector pL4440) construct and the dsRNA targeting
320 different *C. elegans* genes were obtained from the Ahringer RNAi library[22] now available through
321 Source Bioscience. All RNAi clones used in experiments were sequenced for verification before
322 use. For RNAi experiments, RNAi bacteria with empty (pL4440 vector as control) or the dsRNA-
323 expressing plasmid were grown overnight in LB liquid culture containing ampicillin (100 µg/ml)
324 and then induced with IPTG (1 mM) for 2 hrs before seeding the bacteria on NGM plates
325 supplemented with ampicillin (100 µg/ml) and IPTG (1 mM). Bacterial lawns were allowed to

326 grow 48hr before the start of the experiment. RNAi seeded plates were used for embryo hatch
327 rate experiments or western blot experiments for ubiquitinylated proteins.
328
329 **EMBRYO HATCH RATE**
330 Embryo hatch rate was assessed using 2~5 day-one adult worms, which laid eggs for different
331 durations following NHS or 30min HS, as described previously[20] . After removing mothers,
332 embryos were counted and incubated at 20°C. The number of live progenies were scored after
333 72 hrs. For RNAi experiment, mothers were prepared by transferring them to RNAi plates at L4-
334 stage and allowed to lay eggs for 12 hrs after treatment.
335
336 **WESTERN BLOT**
337 Worm lysates were prepared by boiling samples in Laemmli sample buffer (Bio-Rad; Cat
338 #1610737) with β-mercaptoethanol. For ubiquitinylated protein analysis, about 150 worms were
339 grown on RNAi plates by transferring them 24 hours after bleach hatching from OP50 plate.
340 This was done to bypass embryonic lethality of *smg-1* RNAi. The worms were collected, snap
341 frozen, and lysed by boiling and grinding using a pestle. Lysates were separated on SDS-PAGE
342 (HSP-70: 10%, Ubiquitinylated protein: 12%) and transferred onto nitrocellulose membrane
343 (Bio-Rad; Cat #1620115). Membranes were blocked at RT for 1 hr in Odyssey Blocking Buffer
344 (LI-COR; Cat #927-50000), incubated overnight at 4°C with primary antibodies, and then with
345 IRdye goat anti-mouse IgG 800CW (1:10,000; LI-COR; Cat #926-32210) at RT for 2 hrs.
346 Imaging was performed using the LI-COR Odyssey Infrared System and analyzed with Image
347 Studio software.
348
349 To detect HSP-70 levels, mouse anti-FLAG M2 (1:1000; Sigma-Aldrich; Cat #F3165-1MG) was
350 used to detect HSP-70::FLAG in strains where endogenous *hsp-70* (C12C8.1) was tagged with
351 CRISPR/Cas9. Mouse anti-Ubiquitinylated proteins, clone FK2 (1:1000; Sigma-Aldrich; Cat #04-

352 263), was used to detect ubiquitinylated proteins. For tubulin detection as a loading control,
353 mouse anti-tubulin, clone AA4.3 (1:1000; DSHB; Cat #AB_579793) was used.
354
355 **SMALL RNA INJECTION AND RECOVERY ASSAY**
356 Small RNA was prepared from total RNA extracted from
357 (i) Wild-type animals worms subjected to 30 min HS
358 (ii) *prde-1* animals subjected to 30 min HS
359 Small RNAs were fractionated using the Mirvana miRNA Isolation Kit. The small RNA was then
360 injected at a concentration of 50 ng/µl. Following injection, worms were recovered at 20°C for 2
361 hrs and subsequently maintained under non heat shock conditions (NHS) or subjected to 30
362 mins heat shock at 34°C. Worms were collected in 1x PBS after 6 hrs incubation at 20°C and
363 used for *F44E5.4/.5* mRNA FISH experiment. For RT-qPCR analysis, worms were collected
364 immediately in Trizol, and their RNA harvested as described above.
365
366 **ANALYSIS OF mRNA VARIANTS**
367 To assess whether the loss of piRNAs led to increased transcript errors, we devised a method to
368 identify sequences of individual mRNA molecules prior to the possible incorporation of errors
369 due to PCR amplification. RNA extracted from 3 biological repeats of: wild type *C. elegans* at 30
370 minutes at 34ºC, and *prde-1* at 30 minutes at 34ºC were used. mRNAs were tagged with UMIs
371 using the **SMART-Seq® Total RNA Pico Input with UMIs (ZapR™ Mammalian)**. The UMIs
372 were attached to mRNAs during the first strand-cDNA synthesis, prior to PCR amplification.
373 Subsequently, mRNAs were PCR amplified with 3 cycles of amplification for the initial library
374 PCR and 12 cycles of amplification for the enrichment PCR. Sequencing was performed on the
375 Novaseq 6000; the number paired-end reads sequenced were in the range of 50 million-
376 80million, with a read size of 100 bp.
377

378 Next, data was pre-processed using a modified version of the RNA with UMIs v1.0.16 pipeline[23]
379 and a modified version of the GATK Best Practice: RNA-seq Variant Calling Workflow using the
380 tools from gatk (v4.6.1.0) and Picard (v3.3.0).
381
382 The complete list of relevant tools, and the custom script used are available on github
383 (https://github.com/Prahlad-Lab/umi_celegans_analysis)
384 DOI 10.5281/zenodo.17430104.
385
386 The fastq.gz files required to run this analysis pipeline will be made available through the
387 European Nucleotide Archive (ENA) at EMBL-EBI under accession
388 number PRJEB101605 (https://www.ebi.ac.uk/ena/browser/view/PRJEB101605).
389
390 FastQC [8] was used to check the quality of the FASTQ paired-end reads. The FASTQ files were
391 converted to unmapped bam (uBAM) using gatk FastqToSam tool. Unique molecular identifiers
392 (UMI) were extracted using fgbio ExtractUmifromBam. The UMI were extracted using the
393 parameters indicated in the SMART-Seq® Total RNA Pico Input with UMIs (ZapR™
394 Mammalian) kit, the SMART UMI Adapter from read2 was removed by trimming reads a total of
395 12 nucleotides: “8 nt UMIs + 3 nt UMI linker + 3 nt”. The quality of the uBAM file was measured
396 again with FastQC[8].
397
398 Reads were aligned to genome with STAR[24] (v 2.7.11b) using the *Caenorhabditis elegans*
399 genomic reference and annotation (ENSEMBL WBcel235 version 114)[25]. Per-Sample two pass-
400 mapping was enabled using the option -twopassMode Basic. The main output was an unsorted
401 BAM that included unmapped reads, --outSAMtype was set to "BAM Unsorted" and --
402 outSAMunmapped was set to "Within". A transcriptome-aligned BAM was also output with --
403 quantMode = Transcriptomes SAM. Additional alignment parameters were set to match Encode

404 bulk-rna seq standards --outFilterType = BySJout, --outFilterMultimapNmax = 20, --
405 outFilterMismatchNmax = 999, --alignIntronMin = 20, --alignIntronMax = 1000000, --
406 alignMatesGapMax = 1000000, --alignSJoverhangMin = 8, and --alignSJDBoverhangMin = 1.
407 The number of allowed mismatches were set following the parameter detailed in the BROAD
408 pipeline outFilterMatchNminOverLread = 0.33 --outFilterMismatchNoverLmax = 0.1.
409
410 ***UMI Grouping and Filter***
411 Following alignment, BAM files were sorted by coordinating with Picard SortSam tool. UMI-
412 tools[26] was used to create subgroups based on UMI and sequencing errors within UMIs
413 themselves were corrected. The function umi_tools group was used to output the BAM files and
414 the following options were set : to specify the tag where the UMIs were stored, --extract-umi-
415 method was set to "tag" and --umi-tag was set to "RX" and to output text files with stats about
416 the groups, --group-out = .grouped.tsv The stats text file was used to obtain Family Size of the
417 UMIs and their unique IDs. Around 50% of the reads in all the replicates were Family size =1, as
418 shown in the plot.
419

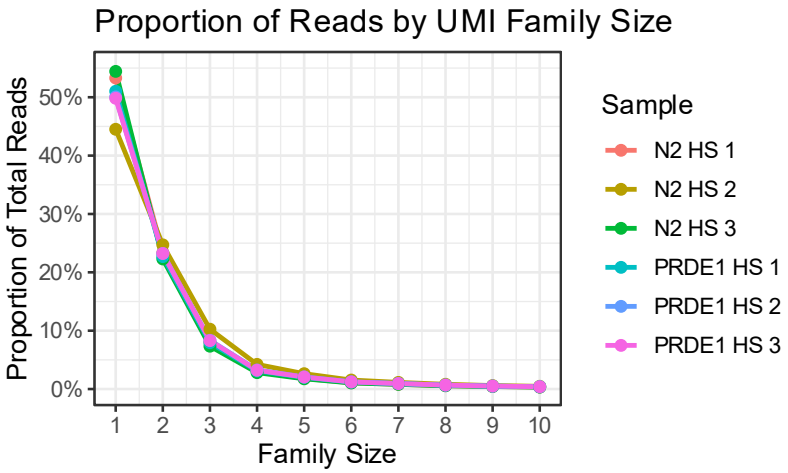

420 Ideally, we would have preferred to generate a consensus from the UMIs families which were in
421 groups >1 (i.e. amplified by PCR), in order to extract the sequence prior to the introduction of
422 PCR errors. However, since 50% (2.7-3.4 x 10^7 individual reads) of the UMI-tagged mRNAs

423 were singletons, i.e. corresponded to the original mRNA sequence and were not PCR amplified,
424 we used these UMIs instead for our analysis (Table 4). Samtools was used to filter and sort the
425 BAM files, using the unique IDs, to keep only the reads a family size of one (Singletons BAM).
426
427 Following the GATK best practices for RNA-seq Variants, the singletons BAM files were
428 processed with gatk SplitNCigarReads to split the reads with "N" in their cigar. To filter out DNA
429 variants, a recalibration model was built with gatk BaseRecalibrator, using Variant Calls from the
430 Caenorhabditis Natural Diversity Resource[27] (CaeNDR) for Hawaiian Strain CB4856
431 (CB4856.hard-filter.vcf.gz) to identify the --known-sites. The resulting model was applied to the
432 singletons BAM files with gatk ApplyBQSR to obtain BSQR BAM.
433
434 ***Pileup Generation and analysis***
435 A pileup of the BSQR BAM was generated with bcftools mpileup using the parameter -d
436 1000000 to get keep the reads at all loci. **To increase confidence that we were detecting**
437 **stochastic mRNA variants, we:**
438 i. analyzed only regions that had generated over 10 reads (i.e. at least 10 mRNAs
439 corresponded to the region to identify the ones which were different). The pileup
440 file was analyzed with a custom python script to filter the regions with total depth
441 <=10 and count the proportion of alternative reads and reference reads.
442 ii. Excluded regions where "Alternative Read/Total Reads =1.0".
443 A custom R script was used to generate tables with the statistics of the Total Number of
444 "mistakes" and the Distribution of the Alternative Reads/Reference reads.
445
446 ***Variant Call and Analysis***
447 HaplotypeCaller was used with the BSQR BAM to call variants and output VCF file. SnpEff [28]
448 was used to annotate the vcf with the SnpEff wbcel235 internal annotation. A custom R script

449 was used to read the VCF and filter the variants with total dept < =10, and SnpEFF Functional
450 Impact type of “Modifier”. Variant Sites with a Ratio of Alternative Read/Total Reads <1.0, were
451 excluded to remove potential genomic Variants. The following were calculated:

452 i. Transcription error rate: Ratio of Alternative Read/Total Reads
453 ii. Deleterious Variant Rates**:** Ratio Deleterious Variants/Total Reads
454 iii. Mismatch Error rate: change in nucleotides type.
455 iv. Transcriptional errors stratified by gene length: protein-coding genes were divided
456 into four quantiles based on their length (from shortest to longest) and then
457 Transcription Error rate was calculated for each quantile. Two sample t-test was used
458 to determine if there was statistical difference between N2 and PRDE1 samples, with
459 p-value=0.05 considered significant.

460

461 **STATISTICAL ANALYSIS**

462 **Statistical analysis (RNA-sequencing data):**

463 Anova with posthoc Tukey HSD was conducted to compare distribution of Gene Length in the
464 Differential Expressed Genes, with adjusted p-value <0.05 was considered significant. Wilcoxon
465 test was used to compare the expression of the piRNAs, difference between the means was
466 considered significant if the p-value <0.05. Hypergeometric test was done using the phyper
467 function in R[29], overlap was considered significant if p-value <0.05. Pearson's Chi-squared test
468 with Yates' correction was used to determine if the number of up- or down-regulated splicing
469 events during heat shock differed between the N2 and PRDE1 strains (p-value <0.05). All the
470 statistical analyses were done in R[29].

471 **Statistical analysis (qPCR data and phenotypes):**

472 The data were analyzed by using Student t-test (two-tailed unpaired t-test) or 2 way-ANOVA
473 (Fisher’s LSD test; GraphPad Prism software) as described in respective figure legends. P
474 values are indicated as follows: $*p < 0.05$; $**p < 0.01$; $***p < 0.001$.

Statistical analysis (other):

The statistical analyses for the remaining datasets are indicated in the Figure Legends.

DATA AVAILABILITY

The data for this study have been deposited in the European Nucleotide Archive (ENA) at EMBL-EBI under accession numbers PRJEB101605 (https://www.ebi.ac.uk/ena/browser/view/PRJEB101605), PRJEB101594 (https://www.ebi.ac.uk/ena/browser/view/PRJEB101594), PRJEB101181(https://www.ebi.ac.uk/ena/browser/view/PRJEB101181) .

REFERENCES

1 Das, S. *et al.* Serotonin signaling by maternal neurons upon stress ensures progeny survival. *Elife* **9** (2020). https://doi.org:10.7554/eLife.55246

2 Tate, A. J., Brown, K. C. & Montgomery, T. A. tiny-count: a counting tool for hierarchical classification and quantification of small RNA-seq reads with single-nucleotide precision. *Bioinformatics Advances* **3** (2023). https://doi.org:10.1093/bioadv/vbad065

3 Chen, S., Zhou, Y., Chen, Y. & Gu, J. fastp: an ultra-fast all-in-one FASTQ preprocessor. *Bioinformatics* **34**, i884-i890 (2018). https://doi.org:10.1093/bioinformatics/bty560

4 Langmead, B., Trapnell, C., Pop, M. & Salzberg, S. L. Ultrafast and memory-efficient alignment of short DNA sequences to the human genome. *Genome Biol* **10**, R25 (2009). https://doi.org:10.1186/gb-2009-10-3-r25

5 Lawrence, M., Gentleman, R. & Carey, V. rtracklayer: an R package for interfacing with genome browsers. *Bioinformatics* **25**, 1841-1842 (2009). https://doi.org:10.1093/bioinformatics/btp328

6 Benjamini, Y. & Hochberg, Y. Controlling the False Discovery Rate: A Practical and Powerful Approach to Multiple Testing. *Journal of the Royal Statistical Society: Series B (Methodological)* **57**, 289-300 (1995). https://doi.org:https://doi.org/10.1111/j.2517-6161.1995.tb02031.x

7 Di Tommaso, P. *et al.* Nextflow enables reproducible computational workflows. *Nat Biotechnol* **35**, 316-319 (2017). https://doi.org:10.1038/nbt.3820

8 Andrews, S. FastQC: A Quality Control Tool for High Throughput Sequence Data (2010). http://www.bioinformatics.babraham.ac.uk/projects/fastqc/

9 Bolger, A. M., Lohse, M. & Usadel, B. Trimmomatic: a flexible trimmer for Illumina sequence data. *Bioinformatics* **30**, 2114-2120 (2014). https://doi.org:10.1093/bioinformatics/btu170

511 10 Cingolani, P. *et al.* A program for annotating and predicting the effects of single
512 nucleotide polymorphisms, SnpEff: SNPs in the genome of Drosophila melanogaster
513 strain w1118; iso-2; iso-3. *Fly (Austin)* **6**, 80-92 (2012). https://doi.org:10.4161/fly.19695
514 11 Garcia-Alcalde, F. *et al.* Qualimap: evaluating next-generation sequencing alignment
515 data. *Bioinformatics* **28**, 2678-2679 (2012). https://doi.org:10.1093/bioinformatics/bts503
516 12 Wang, L., Wang, S. & Li, W. RSeQC: quality control of RNA-seq experiments.
517 *Bioinformatics* **28**, 2184-2185 (2012). https://doi.org:10.1093/bioinformatics/bts356
518 13 Trincado, J. L. *et al.* SUPPA2: fast, accurate, and uncertainty-aware differential splicing
519 analysis across multiple conditions. *Genome Biol* **19**, 40 (2018).
520 https://doi.org:10.1186/s13059-018-1417-1
521 14 Wu, T. *et al.* clusterProfiler 4.0: A universal enrichment tool for interpreting omics data.
522 *Innovation (Camb)* **2**, 100141 (2021). https://doi.org:10.1016/j.xinn.2021.100141
523 15 Yu, G., Wang, L. G., Han, Y. & He, Q. Y. clusterProfiler: an R package for comparing
524 biological themes among gene clusters. *OMICS* **16**, 284-287 (2012).
525 https://doi.org:10.1089/omi.2011.0118
526 16 Carlson, M. org.Ce.eg.db: Genome wide annotation for Worm (2023).
527 DOI: 10.18129/B9.bioc.org.Ce.eg.db
528 https://bioconductor.org/packages/release/data/annotation/html/org.Ce.eg.db.html
529 17 Ramirez, F. *et al.* deepTools2: a next generation web server for deep-sequencing data
530 analysis. *Nucleic Acids Res* **44**, W160-165 (2016). https://doi.org:10.1093/nar/gkw257
531 18 {eulerr}: Area-Proportional Euler and Venn Diagrams with Ellipses v. R package version
532 7.0.2 (2024).
533 19 Wickham, H. ggplot2: Elegant Graphics for Data Analysis. (2016).
534 20 Das, S., Min, S. & Prahlad, V. Gene bookmarking by the heat shock transcription factor
535 programs the insulin-like signaling pathway. *Mol Cell* **81**, 4843-4860 e4848 (2021).
536 https://doi.org:10.1016/j.molcel.2021.09.022

537 21 Das, P. P. *et al.* Piwi and piRNAs act upstream of an endogenous siRNA pathway to
538 suppress Tc3 transposon mobility in the Caenorhabditis elegans germline. *Mol Cell* **31**,
539 79-90 (2008). https://doi.org:10.1016/j.molcel.2008.06.003
540 22 Kamath, R. S. & Ahringer, J. Genome-wide RNAi screening in Caenorhabditis elegans.
541 *Methods* **30**, 313-321 (2003). https://doi.org:10.1016/s1046-2023(03)00050-1
542 23 Degatano, K. *et al.* Warp Analysis Research Pipelines: Cloud-optimized workflows for
543 biological data processing and reproducible analysis. *Bioinformatics* (2025).
544 https://doi.org:10.1093/bioinformatics/btaf494
545 24 Dobin, A. *et al.* STAR: ultrafast universal RNA-seq aligner. *Bioinformatics* **29**, 15-21
546 (2013). https://doi.org:10.1093/bioinformatics/bts635
547 25 Sternberg, P. W. *et al.* WormBase 2024: status and transitioning to Alliance
548 infrastructure. *Genetics* **227** (2024). https://doi.org:10.1093/genetics/iyae050
549 26 Smith, T., Heger, A. & Sudbery, I. UMI-tools: modeling sequencing errors in Unique
550 Molecular Identifiers to improve quantification accuracy. *Genome Res* **27**, 491-499
551 (2017). https://doi.org:10.1101/gr.209601.116
552 27 Crombie, T. A. *et al.* CaeNDR, the Caenorhabditis Natural Diversity Resource. *Nucleic*
553 *Acids Res* **52**, D850-D858 (2024). https://doi.org:10.1093/nar/gkad887
554 28 Cingolani, P. Variant Annotation and Functional Prediction: SnpEff. *Methods Mol Biol*
555 **2493**, 289-314 (2022). https://doi.org:10.1007/978-1-0716-2293-3_19
556 29 R: A Language and Environment for Statistical Computing (2023).
557

Table 1. Strain information

Strain name	Genotype		Source	Note
N2	Bristol N2; Wild-type		CGC	
sx2499	*prde-1(mj207) V*		CGC	
PS3551	*hsf-1 (sy441) I*		CGC	
FLAG::HSF-1	*3X flag::hsf-1 I*	CRISPR /Cas-9	Prahlad Lab	
FLAG::HSF-1 (*sy441*)	*3X flag::hsf-1(sy441) I*	CRISPR /Cas-9	Prahlad Lab	
WM274	*prg-1(tm872) I; neSi14 [FLAG::prg-1 + Cbr-unc-119(+)] II; unc-119(ed3) III.*		CGC	
JDW10	*wrdSi3 [sun-1p::TIR1::F2A::mTagBFP2::AID*::NLS ::tbb-2 3'UTR] II*		CGC	
VP27	*prde-1::AID (syb7464) V*	CRISPR /Cas-9	Prahlad Lab /SunyBiotech	
JDW10 ;VP27	*wrdSi3 [sun-1p::TIR1::F2A::mTagBFP2::AID*::NLS ::tbb-2 3'UTR] II; prde-1::AID (syb7464) V*	Cross	Prahlad Lab	JDW10 was selecte d by picking BFP positive worms
VP01	*C12C8.1::FLAG (syb2141) I*	CRISPR /Cas-9	Prahlad Lab / SunyBiotech	
VP01; sx2499	*C12C8.1::FLAG (syb2141) I; prde-1(mj207) V*	Cross	Prahlad Lab	

Table 2. Primer information

Experiments	Name	Forward	Reverse
genotype	VP01	CTCAAGCTGATATTGATAGA	AGCTAATTGTACAGAGAAAA
	VP27 (Outside AID insertion)	CGTCAAATATGTTGCGCATT	AAAATTCATTCCGCAGCAAC
	VP27 (Inside AID insertion)	GGTTTCCTGCCAAAAATCAA	AAAATTCATTCCGCAGCAAC
	sx2499	GAAATCGCAAAGGACACGAT	CGGCTTGTCACACACAAGAT
Mutliple experiments	*hsp-70 (C12C8.1)* pre-mRNA	TTTATTTTCCGTTTTCAGGTTGA	CCACGTAGGAAGGCGTAGTC
	hsp-70 (C12C8.1) mRNA	TTGGTTGGGGGATCAACTCG	GAGCAGTTGAGGTCCTTCCC
	F44E5.4/.5 pre-mRNA	CGGTACTACGTACTCGTGTGTTG	TGTTATTAAAATTGAAAATGCCAAA
	F44E5.4/.5 mRNA	CTATCAGAATGGAAAGGTTGAG	TCTTTCCGTATCTGTGAATGCC
	pmp-3 mRNA	TAGAGTCAAGGGTCGCAGTG	ATCGGCACCAAGGAAACTGG
PCR for generating Standard Curve	*hsp-70 (C12C8.1)* (cDNA)	CCCGTTGTTGAGGTTGAAGT	CGGCAGCTGATACATTGAGA
	hsp-70 (C12C8.1) (gDNA)	ACGTACTCATGTGTCGGTAT	CGGCAGCTGATACATTGAGA
	F44E5.4/.5 (cDNA)	CTATCAGAATGGAAAGGTTGAG	TCACAAGCAGTTCGGAGACG
	F44E5.4/.5 (gDNA)	TAAAAGGGCTGGGATTCGGG	TCACAAGCAGTTCGGAGACG
	pmp-3 (cDNA)	TGGAGACAGTGGATGTGGAA	GAAAGAACTGTATCGGCACCA
RIP-RT-qPCR	*bath-45* mRNA	ACGATAGGCCTTTTCCAATG	GAGCTGCCTTTTCCAAATTC
ChIP-qPCR	*hsp-70 (C12C8.1)* TSS	ACGTACTCATGTGTCGGTAT	TCTTCTTCCAGTTTACATAATCCT
	hsp-70 (C12C8.1) End	ACAATTCGCAATGAGAAGGGACG	GCATCTTCTGCTGATAACAGTGATC
	F44E5.4/.5 TSS	TAAAAGGGCTGGGATTCGGG	ACCGAGGTCGATACCAATAGC
	F44E5.4/.5 End	TTGATGAAACACTTCGTTGGTTGG	TCCAGCAGTTCCAGGATTTC

RT-qPCR	*T08G5.11*	CGATCAAGAAGGCGGAATCC	TCAACTCGAGACTGCCACAC
	H27M09.6	GCGATCACAAAGGCGGAATC	TCAACTCGAGACTGCCACAC
	F08H9.10	ATCAAGAAGGCGGAATCCCC	TCAACTCGAGACTGCCACAT
	sup-6	TGATCATGAAGACGGAATCCCC	TCAACTCGAGACTGCCACAC
	sup-39	GCCTACCCATTGCACTTTTGG	GCAGCCCCGATACGCAAAA

* Genotyping of sx2499 mutant was verified through digestion with MuCI.

Table 3. Primer information (small RNA)

Experiments	Name	Sequence	Targeting 22G RNA sequence
22G RNA FISH	*F44E5.4/.5* 22G RNA	ATCAGTTTGTCAATCAATTCTC	GAGAATTGATTGACAAACTGAT
sRNA RT-qPCR	*hsp-70 (C12C8.1)* **Stem-loop (SL)**	CTCAACTGGTGTCGTGGAGTCGGCAATTCAGTTGAGTCTATTCG	GCACGTGTGATTTTCGAATAGA
	hsp-70 (C12C8.1) 22G RNA **Forward**	ACACTCCAGCTGGGGCACGTGTGATTTTCG	
	F44E5.4/.5 **Stem-loop (SL)**	CTCAACTGGTGTCGTGGAGTCGGCAATTCAGTTGAGATCAGTTT	GAGAATTGATTGACAAACTGAT
	F44E5.4/.5 22G RNA **Forward**	ACACTCCAGCTGGGGAGAATTGATTGACAA	
	universal **Reverse** primer	CTCAAGTGTCGTGGAGTCGGCAA	
Synthetic RNA	21ur-2348	UGAUGUCCCAUGUCGCAAUUC	

* synthetic 21ur-2348 RNA has 5' phosphorylation at 5' end and 2' O-methyl bases at 3' end

Table 4. UMI total family size 1 (singletons)

sample	family_size	number of reads	proportion
N2 HS 1	1	2.72E+07	0.532974
N2 HS 2	1	3.34E+07	0.445124
N2 HS 3	1	2.79E+07	0.54433
PRDE1 HS 1	1	3.17E+07	0.510223
PRDE1 HS 2	1	3.21E+07	0.500472
PRDE1 HS 3	1	3.20E+07	0.498199